In Vivo Transcriptomic Profiling using Cell Encapsulation Identifies Effector Pathways of Systemic Aging

Omid Mashinchian[1,2,*], Xiaotong Hong[1,3,*], Joris Michaud[1,Ω], Eugenia Migliavacca[1,Ω], Gregory Lefebvre[1], Christophe Boss[1], Filippo De Franceschi[1], Emmeran Le Moal[4], Jasmin Collerette-Tremblay[4], Joan Isern[3], Sylviane Metairon[1], Frederic Raymond[1], Patrick Descombes[1], Nicolas Bouche[1], Pura Muñoz-Cánoves[3,5], Jerome N. Feige[1,2,#], C. Florian Bentzinger[1,4,#]

1. Nestlé Institute of Health Science, Nestlé Research
   Société des Produits Nestlé S.A.
   Lausanne, Switzerland
2. School of Life Sciences
   École Polytechnique Fédérale de Lausanne (EPFL)
   Lausanne, Switzerland
3. Centro Nacional de Investigaciones Cardiovasculares (CNIC), Madrid, Spain
4. Département de Pharmacologie-Physiologie
   Institut de Pharmacologie de Sherbrooke
   Centre de Recherche du Centre Hospitalier Universitaire de Sherbrooke
   Faculté de Médecine et des Sciences de la Santé
   Université de Sherbrooke
   Sherbrooke, Canada
5. Department of Experimental and Health Sciences, Pompeu Fabra University (UPF), CIBER on Neurodegenerative Diseases (CIBERNED) and Institució Catalana de Recerca i Estudis Avançats (ICREA), Barcelona, Spain

*, Ω Equal contribution

# Corresponding authors & equal contribution:
Florian Bentzinger: *cf.bentzinger@usherbrooke.ca*
Jerome Feige: *Jerome.Feige@rd.nestle.com*

Abstract

Sustained exposure to a young systemic environment rejuvenates aged organisms and promotes cellular function. However, due to the intrinsic complexity of tissues it remains challenging to pinpoint niche-independent effects of circulating factors on specific cell populations. Here we describe a method for the encapsulation of human and mouse skeletal muscle progenitors in diffusible polyethersulfone hollow fiber capsules that can be used to profile systemic aging *in vivo* independent of heterogeneous short-range tissue interactions. We observed that circulating long-range signaling factors in the old systemic environment lead to an activation of Myc and E2F transcription factors, induce senescence and suppress myogenic differentiation. Importantly, *in vitro* profiling using young and old serum in 2D culture does not capture all pathways deregulated in encapsulated cells in aged mice. Thus, *in vivo* transcriptomic profiling using cell encapsulation allows for the characterization of effector pathways of systemic aging with unparalleled accuracy.

Main

Systemic crosstalk between tissues has emerged as an important determinant of organismal aging (Demontis et al., 2013). Supporting this notion, several features of tissue aging can be slowed or reversed by heterochronic parabiosis (Bert, 1864; Conboy et al., 2015). Restoration of a youthful systemic environment has been shown to improve the function of muscle, heart, liver, brain, and other tissues in aged mice (Baht et al., 2015; Conboy et al., 2005; Katsimpardi et al., 2014; Loffredo et al., 2013; Ruckh et al., 2012; Sinha et al., 2014; Smith et al., 2015; Villeda et al., 2011). Interestingly, the positive effects of young blood on aged tissues appear to be milder than the pronounced negative effects of aged blood on young tissues (Rebo et al., 2016). This observation suggests the presence of dominant pro-aging factors in the systemic circulation, which cross-talk with local tissue niches to induce the global decline in organ function associated with old age. Recent studies have aimed at identifying the circulating factors involved in systemic aging, and some of the experimental interpretations have led to considerable controversy in the field (Conese et al., 2017).

It has long been known that a range of endocrine hormones are perturbed in later stages of life. Aging affects the somatotroph axis leading to decreased levels of growth hormone and insulin-like growth factor 1 (IGF-1) (Garcia et al., 2000). Levels of sex hormones such as testosterone and estrogen drop in aged individuals (Institute of Medicine, 2004). Old age is also associated with increased systemic inflammation that often goes along with a metabolic syndrome attributed to insulin resistance and an excessive flux of fatty acids (Dominguez and Barbagallo, 2016; Franceschi and Campisi, 2014). Next to these broad biological processes, several distinct pro- and anti-aging factors have been identified in the systemic environment. These include growth differentiation factor 15 (GDF15), eotaxin, β2-microglobulin, and transforming growth factor-β (TGF-β), which negatively affect brain or muscle tissue in aging (Lehallier et al., 2019; Smith et al., 2015; Tanaka et al., 2018; Villeda et al., 2011; Yousef et al., 2015). Factors activating Notch, growth differentiation factor 11 (GDF11) and tissue inhibitor of metalloproteinases 2 (TIMP2), on the other hand, have been suggested to have rejuvenating effects (Castellano et al., 2017; Conboy et al., 2005; Conboy and Rando, 2002; Mahmoudi et al., 2019), although the role of GDF11 is still controversial (Egerman et al., 2015; Egerman and Glass, 2019; Harper et al., 2016; Schafer et al., 2016;

Sinha et al., 2014). In addition, transcript levels of the prolongevity protein Klotho in circulating extracellular vesicles decreases with aging (Sahu et al., 2021).

The modulation of age affected signaling pathways, represents a promising alternative to supplying or inhibiting systemic factors for rejuvenation. However, the study of pathways that are responsive to systemic changes is complicated by the heterogeneous composition of tissues, which contain a multitude of cell types that communicate through secreted short-range signals. Systemic factors do not always act in a direct manner on tissue resident cell populations but can instead trigger paracrine propagation and modulation of signals through accessory cell types in the niche. In the intestinal crypt, paneth cells are known to transmit systemic signals induced by caloric restriction to intestinal stem cells (Yilmaz et al., 2012). Moreover, fibro-adipogenic progenitors, an age-affected support cell population for skeletal muscle stem cells, are highly susceptible to systemic cytokines (Biferali et al., 2019; Lukjanenko et al., 2019). Factors in the aging circulation also alter accessory cell signaling in the neurogenic niche, which contributes to neural stem cell dysfunction (Smith et al., 2018). These examples illustrate that profiling of aging pathways that are directly affected by systemic long-range signaling factors, requires an approach that allows to subtract the pervasive noise generated by the heterogeneous tissue environment.

Here we present a method that allows for the encapsulation of homogeneous cell populations in diffusible hollow fiber capsules that can be transplanted subcutaneously to profile the effects of an aged systemic environment in the absence of short-range cellular interactions (**Fig. 1a**). This approach makes it possible to expose cells from multiple species and different genetic backgrounds to heterotypic physiological environments to characterize gene-environment relationships. It provides a paradigm to disentangle direct effects mediated by systemic signals from cell intrinsic programming and input relayed by accessory cells in the tissue niche.

Encapsulation of myogenic progenitors in PES hollow fiber membranes

Given their wide use in ultra-filtration applications, their oxidative, thermal and hydrolytic stability, and their favorable mechanical properties we chose polyethersulfone (PES) hollow fiber membrane (HFM) tubes for encapsulation of primary human (hskMPs) and C57BL/6J mouse derived skeletal muscle progenitors (mskMPs) (Zhao et al., 2013).

Importantly, PES fibers are biocompatible, have low immunogenicity, and become vascularized when subcutaneously implanted (Hunter et al., 1999). In order to maximize the number of encapsulated cells and, at the same time, allow for adequate oxygen diffusion throughout the capsule, we selected a tubular HFM with an outer diameter of 0.9 mm and an inner diameter of 0.7 mm (**Fig. 1b**). The spongy-like, cross-linked architecture of PES-HFM allows for the diffusion of molecules up to 280 kDa freely through the membrane but prevents infiltration by cells. To provide a suitable adhesion matrix, cells were embedded in growth factor reduced Matrigel (Kleinman et al., 1982). Based on flow cytometric quantification of apoptosis, Matrigel resulted in cellular viability >90% following a ten-day culture period that was superior to other extracellular matrix substrates or hydrogel (**Supplementary Fig. 1a-c**)**.** After mounting of the HFM to an adaptor hub, the exposed end and the external hub interface were sealed using a bio-compatible photopolymerizing medical grade polyacrylate adhesive (**Fig. 1c and Supplementary Fig. 1d**). Sealing of devices was verified using a submersion air pressure decay test. Trypsinized hskMPs or mskMPs mixed with Matrigel were injected into the capsule trough the adaptor hub and the loaded capsule was transferred onto a 3D printed autoclavable USP Class VI plastic cutting and sealing platform (**Supplementary Fig. 1e,f**). Following cutting of the adaptor hub, the loaded capsule remained protected in the UV impermeable plastic device while the second adhesive seal was photopolymerized.

In vitro **characterization of encapsulated myogenic progenitors**

For validation of our experimental setup and to interrogate the behavior of encapsulated cells, we performed a series of *in vitro* experiments. Capsules loaded with hskMPs or mskMPs were placed into culture dishes, immersed in growth media, and were maintained on a horizontal shaker platform in a tissue culture incubator. Terminal deoxynucleotidyl transferase dUTP nick end labeling (TUNEL) staining of cryosections from capsules that were kept in culture for ten days revealed that over 90% of the cells remained viable (**Fig. 2a,b**)**.** Indicative of proper oxygen and nutrient supply, cell density increased slightly in capsules in culture (**Fig. 2c,d**). Following ten days in culture, hskMPs and mskMPs were distributed across the entire diameter of the capsules (**Fig. 2e,f**). Over the ten-day encapsulation time-course, hskMPs and mskMPs showed a mild ≤37% reduction in the number of cells positive for the myogenic marker Pax7, while ≥80% of the cells remained

positive for MyoD (**Fig. 2g-l**). Indicating that the capsule 3D context favors the maintenance of myogenic markers, hskMPs in classic 2D culture downregulated Pax7 and MyoD expression by 62% and MyoD by 37% over the same ten-day period (**Supplementary Fig. 1g**). No apparent difference in the distribution of mitochondria was observed when hskMPs or mskMPs in 2D culture were compared to encapsulated cells (**Supplementary Fig. 2a-d**). When compared to cells in 2D culture, 3D exposure to Matrigel in the capsules led to a higher cytoskeletal complexity with an 123% increase in filopodia in mskMPs (**Supplementary Fig. 2a-e**). Growth factor deprivation over a four-day differentiation period, induced a robust ≥80% reduction of Pax7 in hskMPs and mskMPs, reduced MyoD by 43% in human cells, and, in spite of spatial restraints due to 3D embedding, increased the terminal differentiation marker myosin heavy chain (MHC) by ≥170% in both cell types (**Fig. 2m-s**)**.** After encapsulation, proliferative cells could be recovered from the capsules by enzymatic liberation (**Supplementary Fig. 3a**). Collectively, these observations demonstrate that encapsulated hskMPs and mskMPs remain viable and proliferative, retain the expression of myogenic markers, and are capable to respond to pro-differentiative signals.

In vivo **characterization of encapsulated myogenic progenitors**

We next established the capsule implantation and recovery procedure in adult male C57BL/6J mice. Since it is easily accessible and in contact with the extensive subcutaneous vasculature, skeletal muscle, and bone, resembling the systemic environment myogenic progenitors are exposed to *in situ*, we chose the myofascia of the ribcage as an implantation site. The animals were anesthetized, and incisions were made on the back slightly posterior to each scapula. Three to four capsules containing hskMPs or mskMPs were introduced in varying locations into the subcutaneous fascia over the ribcage separated by 3-5 mm (**Fig. 3a**). Capsule insertion was performed using a hypodermal plastic tube with a sliding metal plunger. In case of hskMPs, an immune reaction to secreted xenogeneic proteins was prevented by subcutaneous implantation of an osmotic pump supplying the immunosuppressant FK-506 on the flank contralateral to the capsules. After ten days of *in vivo* insertion the capsules showed external vascularization and minimal connective tissue build-up (**Fig. 3b**). The porous capsule wall served as an effective barrier for host cells, and we did not observe any CD31 positive blood vessels that were able to penetrate the devices

(**Supplementary Fig. 3b).** TUNEL apoptosis assays using cross-sections from explanted capsules revealed that ≥80% of hskMPs and mskMPs remained viable (**Fig. 3c,d**), and that Pax7, MyoD and MHC were still expressed by the cells (**Fig. 3e-m**). Out of a panel of 40 inflammatory markers, not a single factor was upregulated in serum from C57BL/6J mice that received capsules containing syngeneic cells in the absence of immunosuppression (**Supplementary Fig. 4a and Supplementary Table 1**). Thus, PES hollow fiber capsules do not cause an apparent immunogenic response.

In vivo profiling of systemic aging

To apply our systemic profiling protocol, we implanted young and aged C57BL/6J mice with capsules containing hskMPs and mskMPs. hskMPs take about ten days to fully fuse into myotubes (Cheng et al., 2014). Thus, in order to account for eventual differentiative effects of the systemic environment on the encapsulated cells, we chose this time point for isolation and analysis. The RNA yield was sufficient for genome wide transcriptomic profiling for both cell types (**Supplementary Fig. 5a,b**). Gene set enrichment analysis using the hallmark database revealed that targets of the Myc and E2F family of transcription factors that have previously been implicated in aging and senescence, were induced in both hskMPs and mskMPs exposed to an aged systemic environment (Dimri et al., 2000; Hofmann et al., 2015; Shavlakadze et al., 2018) (**Fig. 4a-c and Supplementary Table 2-5**). To confirm these findings independently, we performed semi-quantitative PCR using mRNA isolated from capsules containing hskMPs after ten days of implantation in young and aged mice. This experiment confirmed age-mediated a 157% increase of the Myc target small nuclear ribonucleoprotein polypeptide A' (Snrpa1) and a 92% increase of the E2F target transferrin receptor (Tfrc) that were part of the respective gene sets upregulated in encapsulated cells in old mice (**Supplementary Fig. 5c,d**).

Myc is induced by mitogens and inflammatory processes (Frank et al., 2001; Liu et al., 2015). However, aging is known to downregulate systemic sex hormones and the somatotroph axis leading to decreased levels of critical growth factors and mitogens such as IGF-1 and growth hormone (Garcia et al., 2000). Thus, in order to determine whether Myc induction goes along with elevated systemic proinflammatory markers, we profiled serum from aged C57BL/6J mice and detected increased levels of B lymphocyte chemoattractant

(BLC, CXCL13), intercellular adhesion molecule-1 (ICAM-1, CD54), Leptin, monokine induced by gamma (MIG, CXCL9) and TIMP-1 when compared to the young condition (**Supplementary Fig. 6a and Supplementary Table 6**). Interestingly, immunostaining for Ki-67 showed that increased levels of Myc signaling in the aged condition did not lead to a higher rate of proliferation in encapsulated cells (**Supplementary Fig. 7a,b**). However, we observed an 39% increase in β-galactosidase positive senescent cells in capsules explanted from aged mice (**Supplementary Fig. 7c,d**).

Further gene set analysis revealed that the categories myogenesis, epithelial–mesenchymal transition (EMT), interleukin, interferon, and p53 signaling were found to be suppressed in hskMPs and mskMPs by an aged systemic environment (**Fig. 4d and Supplementary Table 7,8**). In agreement with an anti-myogenic effect in the aged circulation, we observed that encapsulated hskMPs explanted from old mice showed a 51% lower fusion index than in the young condition (**Supplementary Fig 7e,f**).

To determine which features of aging are directly controlled by long-range secreted factors in the systemic circulation as opposed to signals transduced by the physiological tissue niche, we compared our dataset to freshly isolated myogenic progenitors from young and aged C57BL/6J mice (**Fig. 4e and Supplementary Table 9,10**). Next to many exclusively niche controlled processes, we observed an overlap with respect to an upregulation of Myc and E2F targets, as well as a downregulation of myogenesis and EMT. Collectively, these results demonstrate that aging is characterized by an increased abundance of systemic inflammatory molecules that correlates with higher activity of Myc and E2F transcription factors, cellular senescence, and a reduced differentiation potential of myogenic progenitors.

Exposure to aged serum only captures a fraction of systemically affected pathways

We next set out to determine whether the systemic aging signature we observed using encapsulated cells *in vivo* can be reproduced using a simple cell culture paradigm. To this end we exposed hskMPs in 2D culture for four and ten days to young and aged human serum, isolated RNA, and performed and genome wide transcriptomic profiling. Gene set enrichment analysis revealed that aged human serum led to a weak induction of pathways at day four, while more gene categories and a partial overlap with the profile obtained from

encapsulated myogenic progenitors in old mice was observed at day ten (**Supplementary Fig. 8a and Supplementary Table 11,12**). In particular, the top three pathways, Myc targets, oxidative phosphorylation, and E2F targets, were similarly induced by aged human serum *in vitro* and in encapsulated myogenic progenitors in old mice. Counterintuitively, the category myogenesis was upregulated by aged serum *in vitro* after both four and ten days of exposure. Moreover, other gene set categories such as fatty acid metabolism that were strongly induced in both encapsulated cells in old mice and in aged freshly isolated myogenic progenitors, were not affected by aged serum *in vitro*.

After both four or ten days of exposure of hskMPs to aged human serum *in vitro*, we observed a robust response in downregulated gene sets (**Supplementary Fig. 8b and Supplementary Table 13,14**). However, in particular the top downregulated gene sets showed poor overlap with the profile obtained from encapsulated hskMPs or mskMPs in aged mice or in freshly isolated old myogenic progenitors. Moreover, myogenesis, which was consistently downregulated in both encapsulated cells and in freshly isolated cells in the aged condition, was not repressed by aged serum *in vitro*.

In contrast to our observations using encapsulated cells (**Supplementary Fig. 7a-f**), we observed that aged human serum *in vitro* did not increase the abundance of senescence-associated beta-galactosidase positive cells or affect the fusion index of the cells (**Supplementary Fig. 9a-f**). Overall, these results demonstrate that the effects of systemic aging observed in encapsulated myogenic progenitors in old mice can only partially be reproduced *in vitro*.

We conclude that cell encapsulation allows to capture the transcriptional effects of systemic aging on myogenic progenitors at unprecedented resolution. Long-range signals in the aged circulation lead to a deregulation of a wide variety of pathways, including an activation of Myc and E2F transcription factors, as well as an induction of anti-myogenic and senescence related processes.

Discussion

Our study demonstrates that encapsulation of syn- and xenogeneic cells allows for systemic transcriptional profiling independent of short-range heterogenous cellular interactions. The effects of aged serum on cells in 2D culture only partially overlapped with our observations in encapsulated cells in young and old mice. This result supports the notion that certain factors in the systemic circulation are unstable *in vitro* or have a very short half-life. Compared to other types of capsules that have been used in mice, for instance planar macroencapsulation devices (Lathuiliere et al., 2014), hollow fiber capsules are miniaturized to a diameter of 0.7 mm and a length of 1cm that can be varied according to need. PES is one of the most frequently used polymers in medical applications and, due to its low immunogenicity, has been studied extensively in the context of artificial organs and medical devices used for blood purification in humans (Samtleben et al., 2003; Tullis et al., 2002; Werner et al., 1995; Zhao et al., 2001). Underlining its biocompatibility, we observed that subcutaneous implantation of PES capsules did not induce systemic inflammatory markers.

The myofascia of the ribcage is extensively vascularized and in close proximity to bone and skeletal muscle. Thus, resembling the endogenous niche environment of myogenic cells, it was well suitable as an implantation site for our study. However, for investigation of other cell types that require implantation in different tissues or organs the hollow fiber capsule format may not be ideal and may have to be adapted. Further miniaturization of the capsules would likely yield insufficient mRNA for bulk transcriptomics and either extensive amplification or single-cell sequencing would be required for downstream processing. Given, the broad interest of the aging field in using skeletal muscle stem cells as a model system for tissue maintenance and repair (Drew, 2018; Evano and Tajbakhsh, 2018; Gopinath and Rando, 2008), we selected myogenic progenitors for our profiling experiments. We observed that after explantation of capsules viable proliferative cells can be enzymatically liberated. Thus, our method is not limited to bulk transcriptomic profiling, but could also be modified to allow for single cell sequencing or for the *in vitro* study of long-lasting intrinsic adaptations induced by exposure to an aged systemic environment.

Worldwide, the population of aged individuals has grown to an unprecedented size, and by 2050 more than 430 million people will be over the age of 80 (Drew, 2018). The characterization of *bona fide* aging signatures in defined cell populations independent of the

heterogenous niche context, could potentially allow for the identification of novel therapeutic targets for the systemic treatment of age-associated cellular dysfunction in frail individuals. Importantly, cell encapsulation allows to filter out the dominant noise of the aged tissue that is in direct contact with the cell population of interest. Only long-range signaling factors are able to diffuse over the capsule membrane, which allows to read out effects of these molecules independent of extracellular matrix, heterologous cell-cell contacts, and short-range paracrine growth factors secreted by accessory cells in the tissue. Therefore, in contrast to profiling of cells directly extracted from aged niches or following parabiotic pairing, encapsulation allows to obtain a pure and unbiased transcriptional signature of the systemic environment in defined cell types of choice and makes this amenable to cellular signaling across different species. As such, encapsulation is not an alternative to studying cells in their endogenous niche, but a complementary approach that allows to dissect specific questions on systemic versus tissue-mediated interactions.

Using gene set enrichment analysis, we observed that the aged systemic environment induces senescence, is anti-myogenic, and activates the Myc and E2F family of transcription factors in both mouse and human myogenic progenitors. E2F1, which interacts with the retinoblastoma tumor suppressor, has been shown to have a role in promoting cellular senescence (Dimri et al., 2000). Mice haploinsufficient for Myc exhibit an increased lifespan and are resistant to osteoporosis, cardiac fibrosis and immunosenescence (Hofmann et al., 2015). Rapalogs, which inhibit the activity of mammalian target of rapamycin complex 1, increase life span and delay hallmarks of aging in many species. It has been shown that the rapalog RAD001, counter-regulates Myc in aged kidneys (Shavlakadze et al., 2018). Moreover, Myc is known to be induced by mitogens and inflammatory processes (Frank et al., 2001; Liu et al., 2015). In agreement with these observations, we detected significantly increased levels of systemic pro-inflammatory factors in aged mice. Interestingly, fundamental biological mechanisms such as RNA processing and inflammation related processes affected in our encapsulation study, were also changed in brain tissue of heterochronic parabionts (Baruch et al., 2014). Altogether, our study suggests that these cellular mechanisms are a consequence of systemic aging that occur independent of the influence of heterologous tissue-resident accessory cells. In contrast, comparison to myogenic cells directly isolated from skeletal muscle tissue, indicates that processes such as

apoptosis are imposed by the aged niche and are not directly affected by the systemic environment.

Importantly, our protocol is not limited to aging and might also allow to assess the impact of other multisystemic conditions on defined cell populations of interest. Moreover, in future applications, the combination of encapsulation technology with genetically engineered or induced pluripotent stem cell (iPSC) derived cells, could allow to study systemic effects under controlled physiological conditions at an unprecedented level of detail.

Acknowledgements

We are grateful to Nagabhooshan Hegde, José Sanchez and the Nestlé Institute of Health Science Musculo-Skeletal Health and Cell Biology departments and community for discussion and support. We thank Phoukham Phothirath and Oliver Rizzo of the preclinical investigations group of Nestlé Research for expert advice and support with *in vivo* experiments. O.M., J.N.F. and C.F.B are supported by the Fondation Suisse de Recherche sur les Maladies Musculaires (FSRMM). C.F.B. is supported by the Canadian Institutes of Health Research (CIHR, PJT-162442), the Natural Sciences and Engineering Research Council of Canada (NSERC, RGPIN-2017-05490), the Fonds de Recherche du Québec - Santé (FRQS, Dossiers 296357, 34813, and 36789), the ThéCell Network (supported by the FRQS), the Canadian Stem Cell Network, and a research chair of the Centre de Recherche Médicale de l'Université de Sherbrooke (CRMUS). P.M.C is supported by ERC-2016-AdG-741966, La Caixa-HEALTH-HR17-00040, MDA, AFM, MWRF, UPGRADE-H2020-825825, RTI2018-096068-B-I00, a María de Maeztu Unit of Excellence award to UPF (MDM-2014-0370), and a Severo Ochoa Center of Excellence award to the CNIC (SEV-2015-0505). X.H is recipient of a Severo Ochoa FPI (SEV-2015-0505-17-1) predoctoral fellowship.

Author Contributions

O.M., X.H., C.B., F.D.F., J.M., and N.B. contributed to experimental design, conducted experiments, and analyzed results. E.LM., J.C.T, J.I., and P.M.C. provided critical reagents and experimental support. E.M. and G.L. performed bioinformatic analysis. S.M., F.R. and P.D. developed the RNA isolation methodology and performed transcriptional profiling. O.M., X.H., J.N.F, and C.F.B. directed the study, designed experiments, analyzed and interpreted results, and wrote the manuscript.

Competing Financial Interests

O.M., X.H., E.M., G.L., C.B., F.D.F., J.M., S.M., F.R., P.D., N.B., J.N.F. and C.F.B. were or are employees of the Société des Produits Nestlé S.A., Switzerland.

Figure legends

Fig. 1 | PES hollow fiber capsules for transcriptomic profiling of long-range systemic signals. a, Scheme outlining interactions in the tissue niche in the context of the systemic circulation. Using cell encapsulation, the direct effects of long-range diffusible factors, including growth factors, nutrients, gases and ions, on maintenance and differentiation of defined cell types of interest can be assessed independent of the influence of accessory cells presenting cell-cell adhesion receptors or secreting extracellular matrix and short-range signaling factors. **b**, Scanning electron micrographs of the polyethersulfone (PES) hollow fiber membrane. Scale bars: 200 µm (top left), 20 µm (bottom left) and 5 µm (right). **c**, Schematic outlining the capsule loading procedure and photograph of a PES hollow fiber membrane mounted to the adaptor hub.

Fig. 2 | *In vitro* characterization of encapsulated myogenic progenitors. a,**b**, Terminal deoxynucleotidyl transferase dUTP nick end labeling (TUNEL) based quantification of apoptosis in encapsulated human (hskMP) or mouse (mskMP) skeletal muscle progenitors maintained in growth media for ten days. **c**,**d** DNA staining based quantification of hskMP or mskMP numbers in cross sections of capsules maintained for 4, 8 or 10 days in growth media. **e**,**f**, Representative DNA stainings of cross sections from a capsule containing hskMPs or mskMPs maintained ten days in growth media. Scale bars: 75 µm. **g**, Representative Pax7 immunostainings of cross sections from capsules containing hskMPs or mskMPs maintained ten days in growth media. Scale bars: 150 µm. **h**,**i**, Quantification of Pax7 positive cells in capsules containing hskMPs or mskMPs maintained for 4, 8 or 10 days in growth media. **j**, Representative MyoD immunostainings of cross sections from capsules containing hskMPs or mskMPs maintained ten days in growth media. Scale bars: 150 µm. **k**,**l**, Quantification of MyoD positive cells in capsules containing hskMPs or mskMPs maintained for 4, 8 or 10 days in growth media. **m-p**, Quantification of Pax7 and MyoD in cross sections from capsules maintained for four days under proliferative (Prolif.) conditions in growth media or in differentiation (Diff.) media. **q**, Representative myosin heavy chain (MHC) immunostainings of cross sections from capsules containing hskMPs or mskMPs maintained for four days in differentiation media. Scale bars: 75 µm. **r**,**s**, Quantification of MHC positive cells in capsules containing hskMPs or mskMPs maintained for four days in growth media

compared to differentiation media. All graphs represent means +/- s.e.m. n≥3 cross sections from different capsules were quantified for each experiment and time-point. ****P<0.0001, ***P<0.001, **P<0.01, *P<0.05. Two-way comparisons were made with a student's t–test and multiple comparisons by one–way ANOVA followed by Bonferroni post–test.

Fig. 3 | *In vivo* characterization of encapsulated myogenic progenitors. a, Schematic of the implantation strategy for the PES hollow fiber capsules in mice. In case of hskMPs, an osmotic pump supplying immunosuppressant was implanted at the contralateral flank. **b**, Photograph of the capsules in the connective tissue under the skin of mice ten days after implantation. Arrows are pointing at blood vessels in proximity of the capsules. Scale bar: 0.2 cm. **c**,**d**, Quantification of TUNEL negative hskMP or mskMP skeletal muscle progenitors after ten days *in vivo*. **e**, Representative Pax7 immunostainings of cross sections from capsules containing hskMPs or mskMPs after ten days *in vivo*. **f**,**g**, Quantification of Pax7 positive cells in capsules containing hskMPs or mskMPs after ten days *in vivo*. **h**, Representative MyoD immunostainings of cross sections from capsules containing hskMPs or mskMPs after ten days *in vivo*. **i**,**j**, Quantification of MyoD positive cells in capsules containing hskMPs or mskMPs after ten days *in vivo*. **k**, Representative MHC immunostainings of cross sections from capsules containing hskMPs or mskMPs after ten days *in vivo*. **l**,**m**, Quantification of MHC positive cells in capsules containing hskMPs or mskMPs after ten days *in vivo* (**c**,**d**,**f**,**g**,**i**,**j**,**l**,**m**) Cross sections of capsules explanted from n=3 mice were analyzed for each experiment. Graphs represent means +/- s.e.m. (**e**,**h**,**k**) Scale bars: 150 µm. Comparisons were made by one–way ANOVA followed by Bonferroni post–hoc test.

Fig. 4 | Transcriptomic profiling of systemic aging. a, Gene set enrichment analysis (GSEA) of age-induced genes in encapsulated hskMPs or mskMPs compared to the young control after ten days *in vivo*. Shaded bars represent gene sets overlapping between human and mouse cells. Snowflakes indicate gene sets that are also upregulated by aged serum *in vitro* (Supplementary fig. 8a). **b**,**c**, GSEA barcode plots depicting enrichment of Myc targets with age in encapsulated hskMPs or mskMPs compared to the young control after ten days *in vivo*. **d**, GSEA of genes downregulated with age in encapsulated hskMPs or mskMPs compared to the young control after ten days *in vivo*. Shaded bars represent gene sets

overlapping between human and mouse cells. Snowflakes indicate gene sets that are also downregulated by aged serum *in vitro* (Supplementary fig. 8b). **e**, GSEA of genes up- or downregulated with age in freshly isolated niche resident skeletal muscle stem cells. Shaded bars represent gene sets overlapping with encapsulated hskMPs or mskMPs in young and aged mice. Snowflakes indicate gene sets that are also up- or downregulated by aged serum *in vitro* (Supplementary fig. 8a,b). Data from n=8 young or aged mice. (**a-e**) Samples and data are derived from capsules of n≥5 mice in each age group. False discovery rate (FDR) = Adjusted p-value using Benjamini-Hochberg procedure.

Methods

Cell culture

Human skeletal myoblasts (hskMPs, Lonza, CC-2580) isolated from donated human tissue of 20 year old healthy Caucasians were used at passages 3-5 after obtaining permission for their use in research applications by the Cantonal Ethical Commission of canton de Vaud (CER-VD). For *in vitro* expansion, the cells were maintained in human skeletal muscle myoblast growth medium (Zenbio, SKM-M) in human fibronectin coated dishes fibronectin (Corning, 356008) in a 37°C, 5% CO2 incubator, and were passaged once confluency reached 50%. Primary mouse myoblasts (mskMPs) from 3-week-old C57Bl6/J (Charles River, C57BL/6NCrl) mice were maintained in collagen I coated dishes (Sigma-Aldrich, C3867-1VL) in Ham's F10 media (Wisent, 318-051-CL) containing 20% FBS (Wisent, 80450, lot 115714), 1% Penicillin-Streptomycin solution (Wisent, 450-201-EL) and 2,5 ng/mL bFGF (VWR, 10821-962) in a 37°C, 5% CO2 incubator at a confluence under 80%. For transcriptomic profiling of hskMPs *in vitro*, the cells were seeded into human fibronectin coated dishes (Corning, 356008) in human skeletal muscle myoblast growth medium (Zenbio, SKM-M). After 8 hours, the cells were washed and maintained in medium containing 1% human skeletal muscle myoblast growth medium (Zenbio, SKM-M) and 9% of human serum from 3 different 19-20 year old (young) or 3 different 60-64 year old (aged) healthy Caucasian donors (HumanCells Biosciences, FP-006-C200) after obtaining permission for their use in research applications by informed consent and legal authorization for 4 or 10 days. The cells were maintained under humidified conditions at 37°C in a 5% CO2 incubator and medium was changed every other day.

Embedding of cells

Growth factor reduced Matrigel (Corning, 354230) and MaxGel ECM (Sigma-Aldrich, E0282) were thawed at 4 °C and pipette tips were chilled at -20 °C before starting the experiment. All material was kept on ice or at 4 °C during the procedure. All mixing steps were carried out with caution to avoid generating bubbles. Cells were harvested with trypsin, numbers were quantified using a cell counter (Vi-CELL, AT39233), and the sample was centrifuged. The pellet was resuspended in ice-cold medium at a concentration of 20k cells/µl and kept on ice. The cell mixture was mixed with 1 volume Matrigel or MaxGel by gentle pipetting, giving rise

to a final concentration of 10k cells/µl. Hydrogels (Sigma-Aldrich, TrueGel3D Hydrogel Kit, TRUE7) of ~10kPa were prepared by thawing of the SLO-DEXTRAN solution, TrueGel3D buffer at room temperature. SLO-DEXTRAN solution and TrueGel3D buffer were then mixed with the cells as described above for Matrigel and MaxGel. For hydrogel polymerization peptide based crosslinker (Sigma-Aldrich, TRUECD) was added to the cell suspension mix.

Device mounting

Polyethersulfone (PES) hollow fiber membranes (HFM, AKZO NOBEL) were cut into pieces of 1.2 cm (**Fig. 1b,c**). The adaptor hub (**Supplementary fig. 1d**) was produced by assembling a plastic loading head (Neurotech Pharmaceuticals) with a piece of PEBAX single lumen tubing (Medical Extrusion Technologies). The piece of HFM was then connected to the adaptor hub and sealed at the external interface and the exposed end using a bio-compatible photopolymerizing medical grade adhesive (Loctite, Henkel, L37DAI9124). Polymerization was induced using a BlueWave LED Prime UVA high-intensity spot-curing system (Dymax, 40322) emitting two 5 second pulses of UV. The remaining empty lumen (1 cm) of the capsule holds a volume of 4 µL. Sealing of each device was verified using an air-leak test. While immerged in sterile double distilled water, filtered air was injected at a pressure of 17.58 hPa (2.5 Psi) for 5 s. Devices showing pressure decay greater than 100 Pa over 5 s were discarded. Assembled devices were sterilized with ethylene oxide gas before further use.

Cell encapsulation

10 µl of the cell-Matrigel mixture was loaded into each capsule using a Hamilton gastight syringe (50 µl) through the adaptor hub. Once the injected volume exceeded the inner volume of the device, a fraction of the total volume was ultrafiltrating through the porous membrane. The loaded capsule was transferred onto the 3D printed autoclavable USP Class VI plastic cutting and sealing platform (**Supplementary fig. 1e,f**), cut with a razor blade and sealed with the medical grade adhesive while left protected in the UV blocking plastic device. The capsule was then transferred to pre-warmed media and maintained on a shaker (80 rpm) in a 37° C, 5% CO2 incubator. Media was changed every day. For *in vivo* studies, freshly loaded capsules were maintained in the incubator overnight before implantation. To re-isolate live cells from capsules, they were cut with a razor blade on both ends. A Hamilton gastight

syringe was then used to perfuse with StemPro accutase (Thermo Fisher Scientific, A1110501).

Surgery

Capsule implantation experiments were performed using 6-week to 22-month-old male C57BL/6J mice (Janvier, C57BL/6JRj) in accordance with the Swiss regulation on animal experimentation and the European Community Council directive (86/609/EEC) for the care and use of laboratory animals. Experiments were approved by the Vaud cantonal authorities under license VD3085, and by the Animal Care and Ethics Committee of the Spanish National Cardiovascular Research Center (CNIC) and regional authorities. Mice had access to water and food ad libitum at all time. Animals were randomized by body weight within experimental groups. Before surgery, mice were anesthetized using isoflurane and lidocaine was applied onto the shaved skin. Capsules were implanted through a small incision on the back, slightly posterior to the scapulae. Separated by 3-5 mm, 3-4 capsules were inserted through the incision into the subcutaneous fascia over the rip-cage using hypodermic venflon plastic tube (BD) sliding over a metal plunger. The metal plunger held the capsule in place while the plastic applicator tube was withdrawn over it. For encapsulated human cells, an osmotic minipump (Alzet 1002, Charles River) supplying 2.5 mg/kg/day of FK-506 in 70% ethanol (VWR Chemicals BDH, 153386F) was implanted through a second incision on the opposite side of the spine. Subsequently the incisions were closed using surgical staples. After surgery, mice were kept in single housing with daily surveillance and bodyweight measurement. 10 days after implantation, the mice were euthanized and the capsules were retrieved, washed in warm PBS, incubated in 37 °C warm trypsin for 5 minutes, and washed again before processing. Mice that showed weight loss >15% or displayed signs of wound infection and inflammation, were excluded from the study.

Cryo-sample preparation

Gelatin solution was heated up to and kept at 39 °C until completely melted. Capsules were placed on a layer of gelatin applied to a thin plastic mold. Subsequently, another layer of gelatin was applied to cover the capsules. The sample was then kept at 4 °C for 5 minutes to ensure complete gelation. The sample was then snap frozen in a liquid nitrogen chilled isopentane slurry for 1 minute and transferred to dry ice.

Stainings

Capsule cryosections were fixed with 4% PFA (Thermo Fisher Scientific, 28908). Fixed samples were washed with PBS and permeabilized in 0.1% Triton X-100 (Sigma-Aldrich, T8787) for 15 minutes at room temperature. The sections were then blocked with 4% IgG-free BSA (Jackson ImmunoResearch, 001000162) for 1 hour at room temperature. Samples were incubated with primary antibody at 4°C overnight or for 2 hours at room temperature in blocking buffer. After washing, the sections were incubated with the corresponding secondary antibodies and 40, 6-diamidino-2-phenylindole (Thermo Fisher Scientific, D1306) for 45 minutes at room temperature. After further washing, the slide was dried and mounted (ProLong Diamond Antifade Mountant, P36965). Imaging was carried out using a DMI6000 inverted microscope (Leica, DM14000B) or VS120 slide scanner (Olympus, EVK-L100-042FL). Primary antibodies were anti-Pax7 (DHSB, 528428), anti-MyoD antibody (C-20) (Santa Cruz Biotechnology, sc-304), anti-myosin heavy chain (Merck Millipore, A4.1025), anti-CD31 (Abcam, ab32457), Ki-67 (ab833, Abcam), and anti-β-galactosidase (Abcam, ab9361). Hoechst (B2261, Sigma-Aldrich) was used to stain DNA. Mitochondria were labeled using MitoTracker Red CMXRos (ThermoFisher Scientific, M7512) and F-actin staining was performed using CytoPainter-Phalloidin-iFluor 488 reagent (Abcam, 176753). TUNEL staining was performed using the *In Situ* Cell Death Detection Kit (Roche, 11684795910) according to the manufacturer's instructions.

Fluorescence-activated cell sorting

Cells were isolated after 4 and 10 days of embedding into Matrigel, MaxGel and hydrogel using the TrypLE express enzyme (Thermo Fisher Scientific, 12605010) and StemPro accutase (Thermo Fisher Scientific, A1110501). Cell viability was determined using a LSRFortessa SORP FACS analyzer (BD Biosciences, H647800N0001). CytoCalcein (Pacific Blue) and Apopxin (FITC) (Abcam, ab176749) were used as indicators for live and apoptotic cells. Data was recorded with the BD FACSDiva software version 8.0.2. All data were subsequently analyzed with FCS Express Flow Cytometry version 6.06.0014 (De Novo Software, 4193).

Mouse inflammatory cytokines

Serum cytokines were quantified using the ELISA based Quantibody Mouse Inflammation

Array Q1 Kit (Raybiotech, QAM-INF-1-1). Following incubation of the cytokine-specific immobilized antibodies with serum and standard cytokines, a biotinylated antibody cocktail recognizing the different bound cytokines was added. For detection, Cy3-labelled streptavidin was added, and fluorescence was quantified using the InnoScan 710 AL microarray scanner (Innopsys, Innoscan-710). Data was extracted and computed using MAPIX software (Innopsys, version 8.2.7) and Quantibody Q-Analyzer software (Raybiotech, QAM-INF-1-SW). Cytokine concentration in the samples was determined by comparing signals from unknown samples to the control cytokine standard curve.

RNA extraction and transcriptomic analysis

2-3 devices from the same mouse were pooled and added to a Lysing Matrix D tube (MP Biomedicals, 116913500) on ice. After addition of 450µL of Agencourt RNAdvance Tissue lysis buffer (Beckman Coulter, A32646) the capsules were homogenized using a FastPrep-24 (MP Biomedicals). RNA was extracted using the Agencourt RNAdvance Tissue Kit (Beckman Coulter, A32646) following the manufacturer's instructions. For encapsulated hskMPs, two rounds cRNA synthesis starting with 5 ng of total RNA were performed using the MessageAmp II aRNA amplification kit (Life Technologies, AM1751) and MessageAmp II-biotin enhanced aRNA amplification kit (Life Technologies, AM1791) according to the manufacturer's instructions. RNA and cRNA were quantified using the Quant-iT RiboGreen RNA Assay Kit (Invitrogen, 10207502) using a Spectramax M2 (Molecular Devices, M2). RNA quality assessment was performed using a Bioanalyzer 2100 with RNA 6000 Pico Kit (Agilent Technologies, 5067-1513). cRNA quality assessment was done using a Fragment Analyzer-96 with the Standard Sensitivity RNA Analysis Kit (15-nt) (Advanced Analytical Technologies, DNF-471-0500). Hybridization of 750ng of cRNA on Human HT-12 v4.0 Expression BeadChip (Illumina, BD-103-0604), were performed according to the manufacturer's instructions. Scanning of the microarrays was performed on Illumina HiScan (Illumina, SY-103-1001). No signal was observed on human-specific microarrays using similar amounts of RNA/cRNA from connective tissue isolated in the immediate periphery of the implants. For encapsulated mskMPs, 50 ng of total-RNA was used to generate QuantSeq libraries using the QuantSeq-3’ mRNA-Seq-Library Prep Kit FWD for Illumina (Lexogen, 15.384) following 20 cycles of PCR amplification. Libraries were quantified with the Quant-iT Picogreen (Invitrogen, 10545213) on a FilterMax F3 (Molecular Devices, F3). Size pattern

was assessed with Fragment Analyzer-96 with the DNF-474-0500 High Sensitivity NGS Fragment Analysis Kit (Agilent Technologies, DNF-474-0500). Libraries (Average size: 295 bp) were pooled at an equimolar ratio and clustered at a concentration of 9 pM on a single read sequencing flow cell. 65 cycles of sequencing were performed on an Illumina HiSeq 2500 (Illumina, SY–401–2501) in rapid mode using a 50 cycles SBS Kit (Illumina, GD-402-4002, FC-402-4022) according to the manufacturer's instructions. The generated data were demultiplexed using bcl2fastq v2.19. Reads were aligned to the mouse genome (GRCm38) using STAR (Dobin et al., 2013), and the number of reads mapped within genes was quantified by HTSeq (Anders et al., 2015). Samples had a sequencing depth between 6.9-14.6 million reads, of which between 4.9-10.6 million reads were uniquely mapped. Freshly isolated niche resident cells were isolated and transcriptomically analyzed as previously described (Lukjanenko et al., 2016). Briefly, extracted RNA were subjected to 3′ microarray analysis on Illumina MouseRef–8_V2 chips. Semi-quantitative PCR was performed using a LightCycler 480 (Roche Diagnostics) and the LightCycler DNA green master mix (Roche Molecular Systems, 05573092001). Taqman probes (ThermoFisher Scientific) were Tfrc (Hs00951083_m1), Snrpa1 (Hs00795392_mH) and GAPDH (Hs02758991_g1) as a housekeeper.

3D-printing

Design of the capsule cutting-sealing platform was carried out using Solidworks software (Dassault Systèmes, SW PRO). Printing was done using the ProJet 3500 HDMax (3D systems) 3D printer. VisiJet M3 Crystal and VisiJet S300 (3D systems, 1.0000-M06 and 1.0000-M03) served as printing material and support material, respectively. Schematics are deposited on www.thingiverse.com/thing:4005301**.**

Statistical analysis

After visual inspection and exclusion of microarrays presenting low signal (log2 median expression <6) or low variability (standard deviation <0.1), Illumina expression signals were quantile-normalized. We applied a nonspecific filter to discard probes with low average signal and retained 6969 Illumina probes whose mean expression was greater than the third quartile of expression of all probes. Genes (represented by probes) were tested for differential expression using the moderated t-statistic as implemented in LIMMA(Smyth, 2004). RNA-

sequencing data were normalized by the Trimmed Mean of M-values (TMM) method using the calcNormFactors function in edgeR (Robinson et al., 2010) after selecting genes with more than 4 counts per-million in at least 5 samples. Differentially expressed genes were defined by fitting a quasi-likelihood negative binomial generalized log-linear model to count data using glmQLFTest function in edgeR. The mean-rank gene-set enrichment (Michaud et al., 2008) procedure as implemented in LIMMA was applied to investigate pathway perturbations between gene profiles derived from encapsulated cells exposed to a young and aged environment using the hallmark and C5 (GO) gene set collections from MSigDB (Liberzon et al., 2015) version 6.2. All genome wide statistical analyses were performed using R, version 3.3.3 (microarray data), version 3.5.3 (RNA-sequencing data) and Bioconductor libraries. For cytokine arrays, the mean fluorescence intensities of positive controls were utilized for normalization. Values below the Limit of Detection (LOD) were substituted by LOD/sqrt(2) while the values above the highest standard were replaced by the highest standards. The non-parametric statistical (two-sample Wilcoxon) tests were used for the analysis. For visualization data were log-transformed.

Accession codes

The data discussed in this publication will be deposited in NCBI's Gene Expression Omnibus. GEO Series accession numbers are GSE111401 and GSE81096. The remaining datasets are presently processed.

References

Anders, S., Pyl, P.T., and Huber, W. (2015). HTSeq--a Python framework to work with high-throughput sequencing data. Bioinformatics *31*, 166-169.

Baht, G.S., Silkstone, D., Vi, L., Nadesan, P., Amani, Y., Whetstone, H., Wei, Q., and Alman, B.A. (2015). Exposure to a youthful circulaton rejuvenates bone repair through modulation of beta-catenin. Nat Commun *6*, 7131.

Baruch, K., Deczkowska, A., David, E., Castellano, J.M., Miller, O., Kertser, A., Berkutzki, T., Barnett-Itzhaki, Z., Bezalel, D., Wyss-Coray, T.*, et al.* (2014). Aging. Aging-induced type I interferon response at the choroid plexus negatively affects brain function. Science *346*, 89-93.

Bert, P. (1864). Expériences et Considérations Sur la Greffe Animale. J Anatomie Physiologie *1*, 69–87.

Biferali, B., Proietti, D., Mozzetta, C., and Madaro, L. (2019). Fibro-Adipogenic Progenitors Cross-Talk in Skeletal Muscle: The Social Network. Front Physiol *10*, 1074.

Castellano, J.M., Mosher, K.I., Abbey, R.J., McBride, A.A., James, M.L., Berdnik, D., Shen, J.C., Zou, B., Xie, X.S., Tingle, M.*, et al.* (2017). Human umbilical cord plasma proteins revitalize hippocampal function in aged mice. Nature *544*, 488-492.

Cheng, C.S., El-Abd, Y., Bui, K., Hyun, Y.E., Hughes, R.H., Kraus, W.E., and Truskey, G.A. (2014). Conditions that promote primary human skeletal myoblast culture and muscle differentiation in vitro. Am J Physiol Cell Physiol *306*, C385-395.

Conboy, I.M., Conboy, M.J., and Rebo, J. (2015). Systemic Problems: A perspective on stem cell aging and rejuvenation. Aging (Albany NY) *7*, 754-765.

Conboy, I.M., Conboy, M.J., Wagers, A.J., Girma, E.R., Weissman, I.L., and Rando, T.A. (2005). Rejuvenation of aged progenitor cells by exposure to a young systemic environment. Nature *433*, 760-764.

Conboy, I.M., and Rando, T.A. (2002). The regulation of Notch signaling controls satellite cell activation and cell fate determination in postnatal myogenesis. Dev Cell *3*, 397-409.

Conese, M., Carbone, A., Beccia, E., and Angiolillo, A. (2017). The Fountain of Youth: A Tale of Parabiosis, Stem Cells, and Rejuvenation. Open Med (Wars) *12*, 376-383.

Demontis, F., Piccirillo, R., Goldberg, A.L., and Perrimon, N. (2013). The influence of skeletal muscle on systemic aging and lifespan. Aging Cell *12*, 943-949.

Dimri, G.P., Itahana, K., Acosta, M., and Campisi, J. (2000). Regulation of a senescence checkpoint response by the E2F1 transcription factor and p14(ARF) tumor suppressor. Mol Cell Biol *20*, 273-285.

Dobin, A., Davis, C.A., Schlesinger, F., Drenkow, J., Zaleski, C., Jha, S., Batut, P., Chaisson, M., and Gingeras, T.R. (2013). STAR: ultrafast universal RNA-seq aligner. Bioinformatics *29*, 15-21.

Dominguez, L.J., and Barbagallo, M. (2016). The biology of the metabolic syndrome and aging. Curr Opin Clin Nutr Metab Care *19*, 5-11.

Drew, L. (2018). Fighting the inevitability of ageing. Nature *555*, S15-S17.

Egerman, M.A., Cadena, S.M., Gilbert, J.A., Meyer, A., Nelson, H.N., Swalley, S.E., Mallozzi, C., Jacobi, C., Jennings, L.L., Clay, I.*, et al.* (2015). GDF11 Increases with Age and Inhibits Skeletal Muscle Regeneration. Cell Metab *22*, 164-174.

Egerman, M.A., and Glass, D.J. (2019). The role of GDF11 in aging and skeletal muscle, cardiac and bone homeostasis. Crit Rev Biochem Mol Biol *54*, 174-183.

Evano, B., and Tajbakhsh, S. (2018). Skeletal muscle stem cells in comfort and stress. NPJ Regen Med *3*, 24.

Franceschi, C., and Campisi, J. (2014). Chronic inflammation (inflammaging) and its potential contribution to age-associated diseases. J Gerontol A Biol Sci Med Sci *69 Suppl 1*, S4-9.

Frank, S.R., Schroeder, M., Fernandez, P., Taubert, S., and Amati, B. (2001). Binding of c-Myc to chromatin mediates mitogen-induced acetylation of histone H4 and gene activation. Genes Dev *15*, 2069-2082.

Garcia, J.M., Merriam, G.R., and Kargi, A.Y. (2000). Growth Hormone in Aging. In Endotext, K.R. Feingold, B. Anawalt, A. Boyce, G. Chrousos, K. Dungan, A. Grossman, J.M. Hershman, G. Kaltsas, C. Koch, P. Kopp*, et al.*, eds. (South Dartmouth (MA)).

Gopinath, S.D., and Rando, T.A. (2008). Stem cell review series: aging of the skeletal muscle stem cell niche. Aging Cell *7*, 590-598.

Harper, S.C., Brack, A., MacDonnell, S., Franti, M., Olwin, B.B., Bailey, B.A., Rudnicki, M.A., and Houser, S.R. (2016). Is Growth Differentiation Factor 11 a Realistic Therapeutic for Aging-Dependent Muscle Defects? Circ Res *118*, 1143-1150; discussion 1150.

Hofmann, J.W., Zhao, X., De Cecco, M., Peterson, A.L., Pagliaroli, L., Manivannan, J., Hubbard, G.B., Ikeno, Y., Zhang, Y., Feng, B.*, et al.* (2015). Reduced expression of MYC increases longevity and enhances healthspan. Cell *160*, 477-488.

Hunter, S.K., Kao, J.M., Wang, Y., Benda, J.A., and Rodgers, V.G. (1999). Promotion of neovascularization around hollow fiber bioartificial organs using biologically active substances. ASAIO J *45*, 37-40.

Katsimpardi, L., Litterman, N.K., Schein, P.A., Miller, C.M., Loffredo, F.S., Wojtkiewicz, G.R., Chen, J.W., Lee, R.T., Wagers, A.J., and Rubin, L.L. (2014). Vascular and neurogenic rejuvenation of the aging mouse brain by young systemic factors. Science *344*, 630-634.

Kleinman, H.K., McGarvey, M.L., Liotta, L.A., Robey, P.G., Tryggvason, K., and Martin, G.R. (1982). Isolation and characterization of type IV procollagen, laminin, and heparan sulfate proteoglycan from the EHS sarcoma. Biochemistry *21*, 6188-6193.

Lathuiliere, A., Cosson, S., Lutolf, M.P., Schneider, B.L., and Aebischer, P. (2014). A high-capacity cell macroencapsulation system supporting the long-term survival of genetically engineered allogeneic cells. Biomaterials *35*, 779-791.

Lehallier, B., Gate, D., Schaum, N., Nanasi, T., Lee, S.E., Yousef, H., Moran Losada, P., Berdnik, D., Keller, A., Verghese, J.*, et al.* (2019). Undulating changes in human plasma proteome profiles across the lifespan. Nat Med *25*, 1843-1850.

Liberzon, A., Birger, C., Thorvaldsdottir, H., Ghandi, M., Mesirov, J.P., and Tamayo, P. (2015). The Molecular Signatures Database (MSigDB) hallmark gene set collection. Cell Syst *1*, 417-425.

Liu, T., Zhou, Y., Ko, K.S., and Yang, H. (2015). Interactions between Myc and Mediators of Inflammation in Chronic Liver Diseases. Mediators Inflamm *2015*, 276850.

Loffredo, F.S., Steinhauser, M.L., Jay, S.M., Gannon, J., Pancoast, J.R., Yalamanchi, P., Sinha, M., Dall'Osso, C., Khong, D., Shadrach, J.L.*, et al.* (2013). Growth differentiation factor 11 is a circulating factor that reverses age-related cardiac hypertrophy. Cell *153*, 828-839.

Lukjanenko, L., Jung, M.J., Hegde, N., Perruisseau-Carrier, C., Migliavacca, E., Rozo, M., Karaz, S., Jacot, G., Schmidt, M., Li, L.*, et al.* (2016). Loss of fibronectin from the aged stem cell niche affects the regenerative capacity of skeletal muscle in mice. Nat Med *22*, 897-905.

Lukjanenko, L., Karaz, S., Stuelsatz, P., Gurriaran-Rodriguez, U., Michaud, J., Dammone, G., Sizzano, F., Mashinchian, O., Ancel, S., Migliavacca, E.*, et al.* (2019). Aging Disrupts Muscle Stem Cell Function by Impairing Matricellular WISP1 Secretion from Fibro-Adipogenic Progenitors. Cell Stem Cell.

Mahmoudi, S., Xu, L., and Brunet, A. (2019). Turning back time with emerging rejuvenation strategies. Nat Cell Biol *21*, 32-43.

Medicine, I.o. (2004). Testosterone and Aging: Clinical Research Directions (Washington, DC: The National Academies Press).

Michaud, J., Simpson, K.M., Escher, R., Buchet-Poyau, K., Beissbarth, T., Carmichael, C., Ritchie, M.E., Schutz, F., Cannon, P., Liu, M.*, et al.* (2008). Integrative analysis of RUNX1 downstream pathways and target genes. BMC Genomics *9*, 363.

Rebo, J., Mehdipour, M., Gathwala, R., Causey, K., Liu, Y., Conboy, M.J., and Conboy, I.M. (2016). A single heterochronic blood exchange reveals rapid inhibition of multiple tissues by old blood. Nat Commun *7*, 13363.

Robinson, M.D., McCarthy, D.J., and Smyth, G.K. (2010). edgeR: a Bioconductor package for differential expression analysis of digital gene expression data. Bioinformatics *26*, 139-140.

Ruckh, J.M., Zhao, J.W., Shadrach, J.L., van Wijngaarden, P., Rao, T.N., Wagers, A.J., and Franklin, R.J. (2012). Rejuvenation of regeneration in the aging central nervous system. Cell Stem Cell *10*, 96-103.

Sahu, A., Clemens, Z.J., Shinde, S.N., Sivakumar, S., Pius, A., Bhatia, A., Picciolini, S., Carlomagno, C., Gualerzi, A., Bedoni, M.*, et al.* (2021). Regulation of aged skeletal muscle regeneration by circulating extracellular vesicles. Nature Aging *1*, 1148-1161.

Samtleben, W., Dengler, C., Reinhardt, B., Nothdurft, A., and Lemke, H.D. (2003). Comparison of the new polyethersulfone high-flux membrane DIAPES HF800 with conventional high-flux membranes during on-line haemodiafiltration. Nephrol Dial Transplant *18*, 2382-2386.

Schafer, M.J., Atkinson, E.J., Vanderboom, P.M., Kotajarvi, B., White, T.A., Moore, M.M., Bruce, C.J., Greason, K.L., Suri, R.M., Khosla, S.*, et al.* (2016). Quantification of GDF11 and Myostatin in Human Aging and Cardiovascular Disease. Cell Metab *23*, 1207-1215.

Shavlakadze, T., Zhu, J., Wang, S., Zhou, W., Morin, B., Egerman, M.A., Fan, L., Wang, Y., Iartchouk, O., Meyer, A.*, et al.* (2018). Short-term Low-Dose mTORC1 Inhibition in Aged Rats Counter-Regulates Age-Related Gene Changes and Blocks Age-Related Kidney Pathology. J Gerontol A Biol Sci Med Sci *73*, 845-852.

Sinha, M., Jang, Y.C., Oh, J., Khong, D., Wu, E.Y., Manohar, R., Miller, C., Regalado, S.G., Loffredo, F.S., Pancoast, J.R.*, et al.* (2014). Restoring systemic GDF11 levels reverses age-related dysfunction in mouse skeletal muscle. Science *344*, 649-652.

Smith, L.K., He, Y., Park, J.S., Bieri, G., Snethlage, C.E., Lin, K., Gontier, G., Wabl, R., Plambeck, K.E., Udeochu, J.*, et al.* (2015). beta2-microglobulin is a systemic pro-aging factor that impairs cognitive function and neurogenesis. Nat Med *21*, 932-937.

Smith, L.K., White, C.W., 3rd, and Villeda, S.A. (2018). The systemic environment: at the interface of aging and adult neurogenesis. Cell Tissue Res *371*, 105-113.

Smyth, G.K. (2004). Linear models and empirical bayes methods for assessing differential expression in microarray experiments. Stat Appl Genet Mol Biol *3*, Article3.

Tanaka, T., Biancotto, A., Moaddel, R., Moore, A.Z., Gonzalez-Freire, M., Aon, M.A., Candia, J., Zhang, P., Cheung, F., Fantoni, G.*, et al.* (2018). Plasma proteomic signature of age in healthy humans. Aging Cell *17*, e12799.

Tullis, R.H., Duffin, R.P., Zech, M., and Ambrus, J.L., Jr. (2002). Affinity hemodialysis for antiviral therapy. I. Removal of HIV-1 from cell culture supernatants, plasma, and blood. Ther Apher *6*, 213-220.

Villeda, S.A., Luo, J., Mosher, K.I., Zou, B., Britschgi, M., Bieri, G., Stan, T.M., Fainberg, N., Ding, Z., Eggel, A.*, et al.* (2011). The ageing systemic milieu negatively regulates neurogenesis and cognitive function. Nature *477*, 90-94.

Werner, C., Jacobasch, H.J., and Reichelt, G. (1995). Surface characterization of hemodialysis membranes based on streaming potential measurements. J Biomater Sci Polym Ed *7*, 61-76.

Yilmaz, O.H., Katajisto, P., Lamming, D.W., Gultekin, Y., Bauer-Rowe, K.E., Sengupta, S., Birsoy, K., Dursun, A., Yilmaz, V.O., Selig, M.*, et al.* (2012). mTORC1 in the Paneth cell niche couples intestinal stem-cell function to calorie intake. Nature *486*, 490-495.

Yousef, H., Conboy, M.J., Morgenthaler, A., Schlesinger, C., Bugaj, L., Paliwal, P., Greer, C., Conboy, I.M., and Schaffer, D. (2015). Systemic attenuation of the TGF-beta pathway by a single drug simultaneously rejuvenates hippocampal neurogenesis and myogenesis in the same old mammal. Oncotarget *6*, 11959-11978.

Zhao, C., Xue, J., Ran, F., and Sun, S. (2013). Modification of polyethersulfone membranes – A review of methods. Progress in Materials Science *58*, 76-150.

Zhao, C.S., Liu, T., Lu, Z.P., Cheng, L.P., and Huang, J. (2001). An evaluation of a polyethersulfone hollow fiber plasma separator by animal experiment. Artif Organs *25*, 60-63.

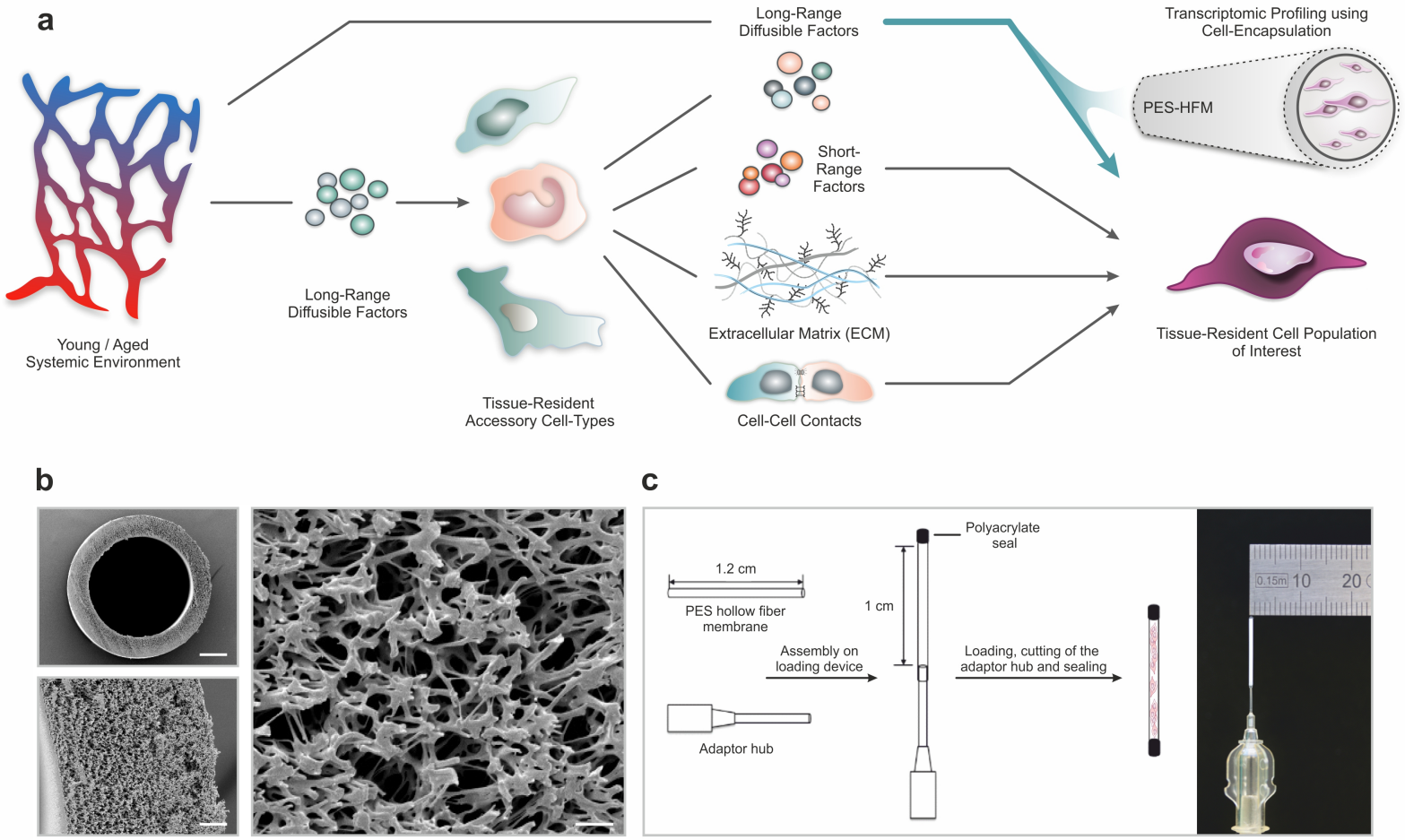
a
Young / Aged
Systemic Environment
Long-Range
Diffusible Factors
Tissue-Resident
Accessory Cell-Types
Long-Range
Diffusible Factors
Short-
Range
Factors
Extracellular Matrix (ECM)
Cell-Cell Contacts
Transcriptomic Profiling using
Cell-Encapsulation
PES-HFM
Tissue-Resident Cell Population
of Interest
b
c
1.2 cm
PES hollow fiber
membrane
Adaptor hub
Assembly on
loading device
1 cm
Polyacrylate
seal
Loading, cutting of the
adaptor hub and sealing
0.15m
10
20

Figure 1

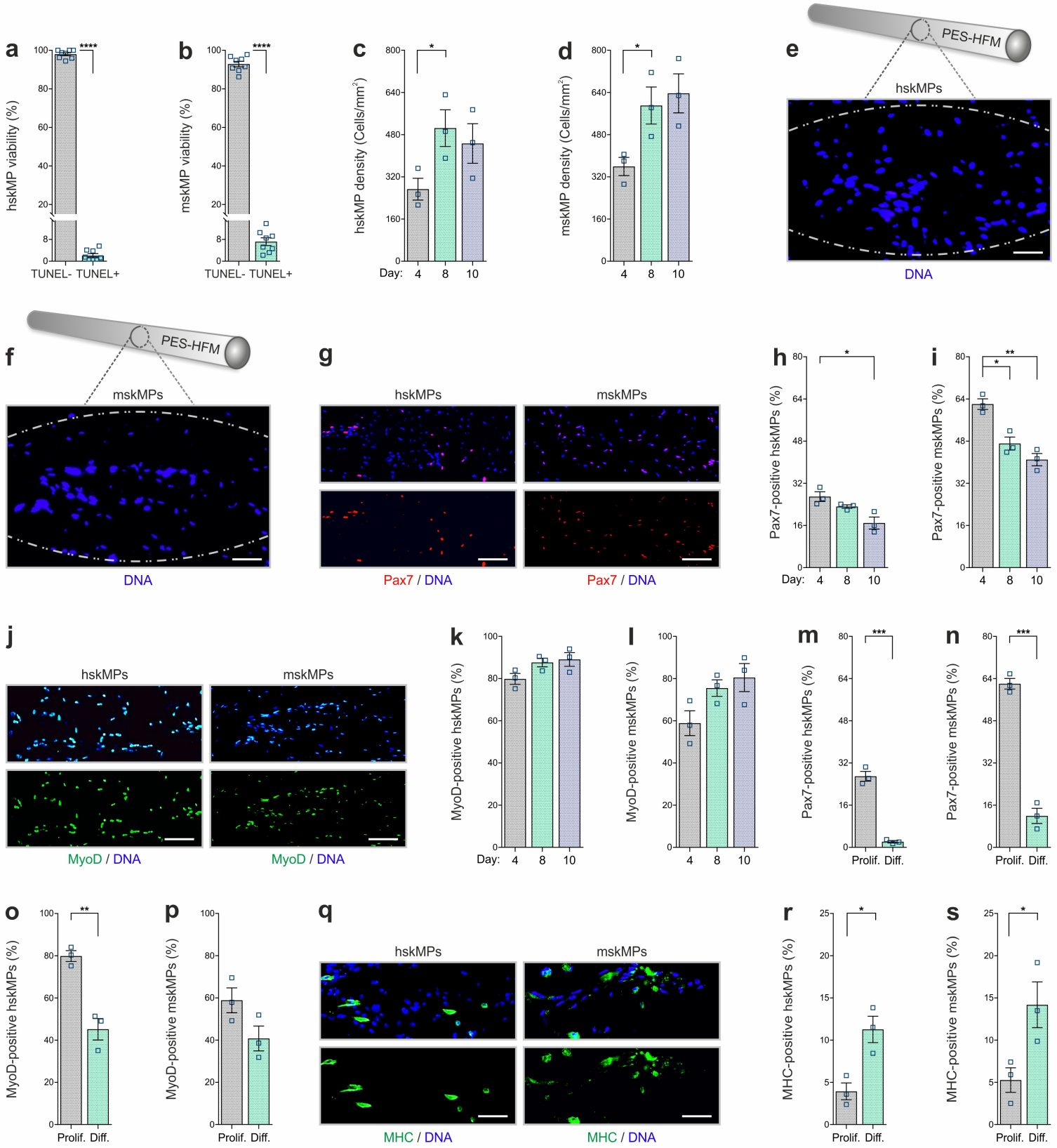
a
hskMP viability (%)
TUNEL-
TUNEL+
****
b
mskMP viability (%)
TUNEL-
TUNEL+
****
c
hskMP density (Cells/mm²)
Day: 4 8 10
*
d
mskMP density (Cells/mm²)
4 8 10
*
e
PES-HFM
hskMPs
DNA
f
PES-HFM
mskMPs
DNA
g
hskMPs
mskMPs
Pax7 / DNA
Pax7 / DNA
h
Pax7-positive hskMPs (%)
Day: 4 8 10
*
i
Pax7-positive mskMPs (%)
4 8 10
**
*
j
hskMPs
mskMPs
MyoD / DNA
MyoD / DNA
k
MyoD-positive hskMPs (%)
Day: 4 8 10
l
MyoD-positive mskMPs (%)
4 8 10
m
Pax7-positive hskMPs (%)
Prolif. Diff.
***
n
Pax7-positive mskMPs (%)
Prolif. Diff.
***
o
MyoD-positive hskMPs (%)
Prolif. Diff.
**
p
MyoD-positive mskMPs (%)
Prolif. Diff.
q
hskMPs
mskMPs
MHC / DNA
MHC / DNA
r
MHC-positive hskMPs (%)
Prolif. Diff.
*
s
MHC-positive mskMPs (%)
Prolif. Diff.
*

Figure 2

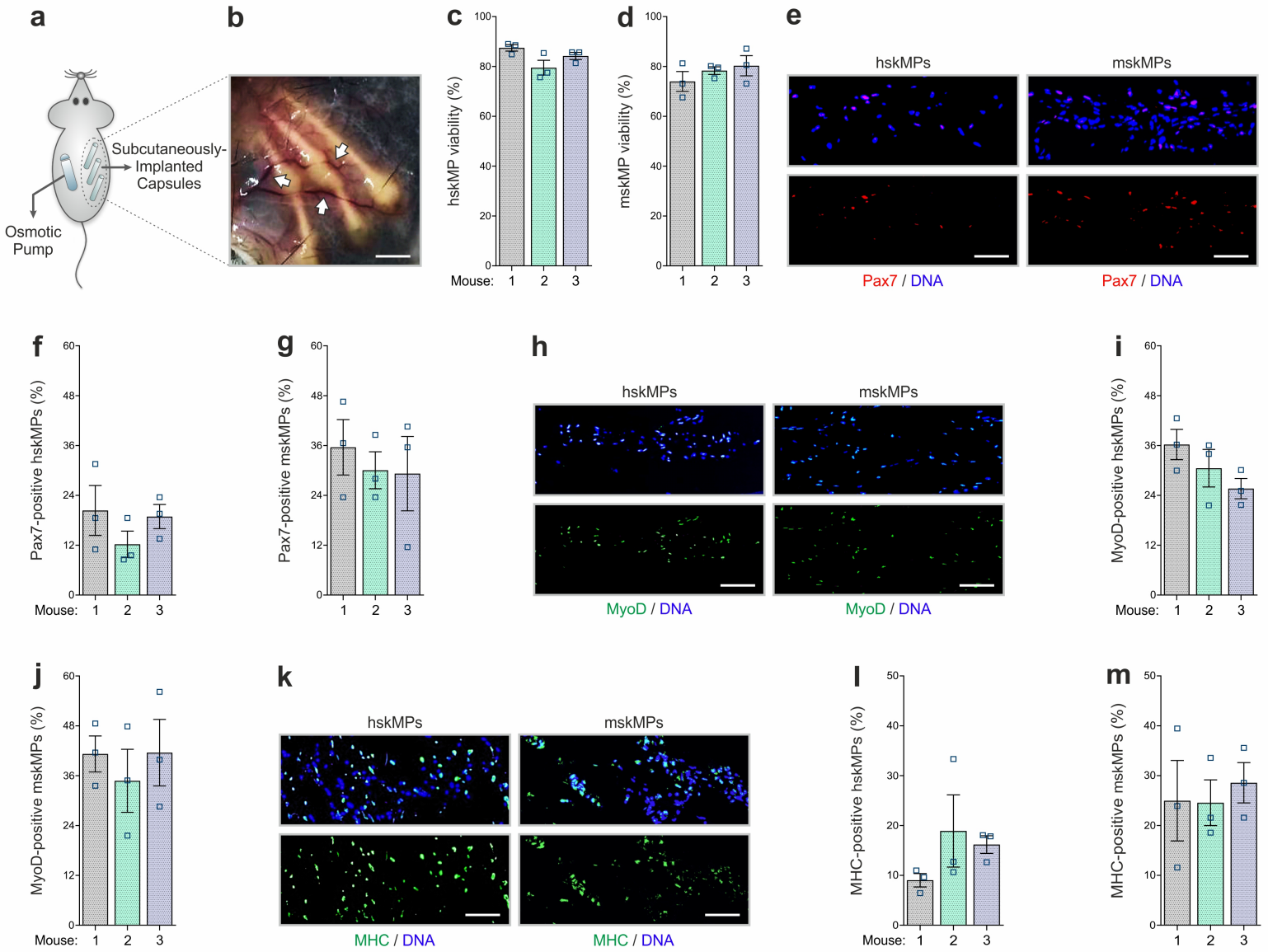
a
Subcutaneously-Implanted Capsules
Osmotic Pump
b
c
hskMP viability (%)
Mouse: 1 2 3
d
mskMP viability (%)
e
hskMPs
mskMPs
Pax7 / DNA
Pax7 / DNA
f
Pax7-positive hskMPs (%)
Mouse: 1 2 3
g
Pax7-positive mskMPs (%)
h
hskMPs
mskMPs
MyoD / DNA
MyoD / DNA
i
MyoD-positive hskMPs (%)
Mouse: 1 2 3
j
MyoD-positive mskMPs (%)
Mouse: 1 2 3
k
hskMPs
mskMPs
MHC / DNA
MHC / DNA
l
MHC-positive hskMPs (%)
Mouse: 1 2 3
m
MHC-positive mskMPs (%)

Figure 3

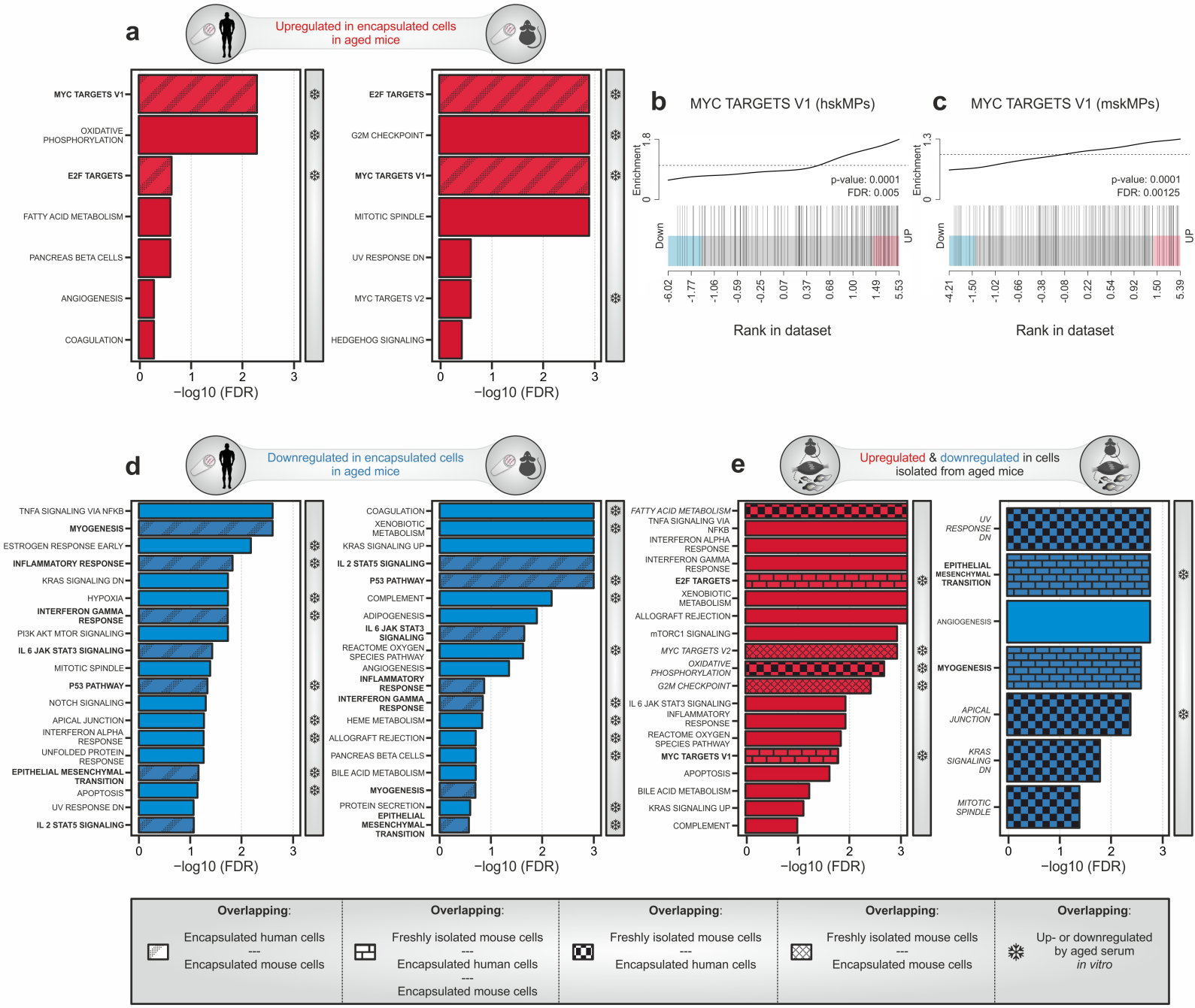
a
Upregulated in encapsulated cells in aged mice
MYC TARGETS V1
OXIDATIVE PHOSPHORYLATION
E2F TARGETS
FATTY ACID METABOLISM
PANCREAS BETA CELLS
ANGIOGENESIS
COAGULATION
E2F TARGETS
G2M CHECKPOINT
MYC TARGETS V1
MITOTIC SPINDLE
UV RESPONSE DN
MYC TARGETS V2
HEDGEHOG SIGNALING
−log10 (FDR)
b
MYC TARGETS V1 (hskMPs)
Enrichment
p-value: 0.0001
FDR: 0.005
Down
UP
Rank in dataset
c
MYC TARGETS V1 (mskMPs)
p-value: 0.0001
FDR: 0.00125
d
Downregulated in encapsulated cells in aged mice
TNFA SIGNALING VIA NFKB
MYOGENESIS
ESTROGEN RESPONSE EARLY
INFLAMMATORY RESPONSE
KRAS SIGNALING DN
HYPOXIA
INTERFERON GAMMA RESPONSE
PI3K AKT MTOR SIGNALING
IL 6 JAK STAT3 SIGNALING
MITOTIC SPINDLE
P53 PATHWAY
NOTCH SIGNALING
APICAL JUNCTION
INTERFERON ALPHA RESPONSE
UNFOLDED PROTEIN RESPONSE
EPITHELIAL MESENCHYMAL TRANSITION
APOPTOSIS
UV RESPONSE DN
IL 2 STAT5 SIGNALING
COAGULATION
XENOBIOTIC METABOLISM
KRAS SIGNALING UP
IL 2 STAT5 SIGNALING
P53 PATHWAY
COMPLEMENT
ADIPOGENESIS
IL 6 JAK STAT3 SIGNALING
REACTOME OXYGEN SPECIES PATHWAY
ANGIOGENESIS
INFLAMMATORY RESPONSE
INTERFERON GAMMA RESPONSE
HEME METABOLISM
ALLOGRAFT REJECTION
PANCREAS BETA CELLS
BILE ACID METABOLISM
MYOGENESIS
PROTEIN SECRETION
EPITHELIAL MESENCHYMAL TRANSITION
e
Upregulated & downregulated in cells isolated from aged mice
FATTY ACID METABOLISM
TNFA SIGNALING VIA NFKB
INTERFERON ALPHA RESPONSE
INTERFERON GAMMA RESPONSE
E2F TARGETS
XENOBIOTIC METABOLISM
ALLOGRAFT REJECTION
mTORC1 SIGNALING
MYC TARGETS V2
OXIDATIVE PHOSPHORYLATION
G2M CHECKPOINT
IL 6 JAK STAT3 SIGNALING
INFLAMMATORY RESPONSE
REACTOME OXYGEN SPECIES PATHWAY
MYC TARGETS V1
APOPTOSIS
BILE ACID METABOLISM
KRAS SIGNALING UP
COMPLEMENT
UV RESPONSE DN
EPITHELIAL MESENCHYMAL TRANSITION
ANGIOGENESIS
MYOGENESIS
APICAL JUNCTION
KRAS SIGNALING DN
MITOTIC SPINDLE
Overlapping:
Encapsulated human cells

Encapsulated mouse cells
Overlapping:
Freshly isolated mouse cells

Encapsulated human cells

Encapsulated mouse cells
Overlapping:
Freshly isolated mouse cells

Encapsulated human cells
Overlapping:
Freshly isolated mouse cells

Encapsulated mouse cells
Overlapping:
Up- or downregulated by aged serum
in vitro

Figure 4

In Vivo Transcriptomic Profiling using Cell Encapsulation Identifies Effector Pathways of Systemic Aging

Omid Mashinchian, Xiaotong Hong, Joris Michaud, Eugenia Migliavacca, Gregory Lefebvre, Christophe Boss, Filippo De Franceschi, Emmeran Le Moal, Jasmin Collerette-Tremblay, Joan Isern, Sylviane Metairon, Frederic Raymond, Patrick Descombes, Nicolas Bouche, Pura Muñoz-Cánoves, Jerome N. Feige, C. Florian Bentzinger

Supplementary Information

Supplementary Figures 1-9

Supplementary Table 1-14

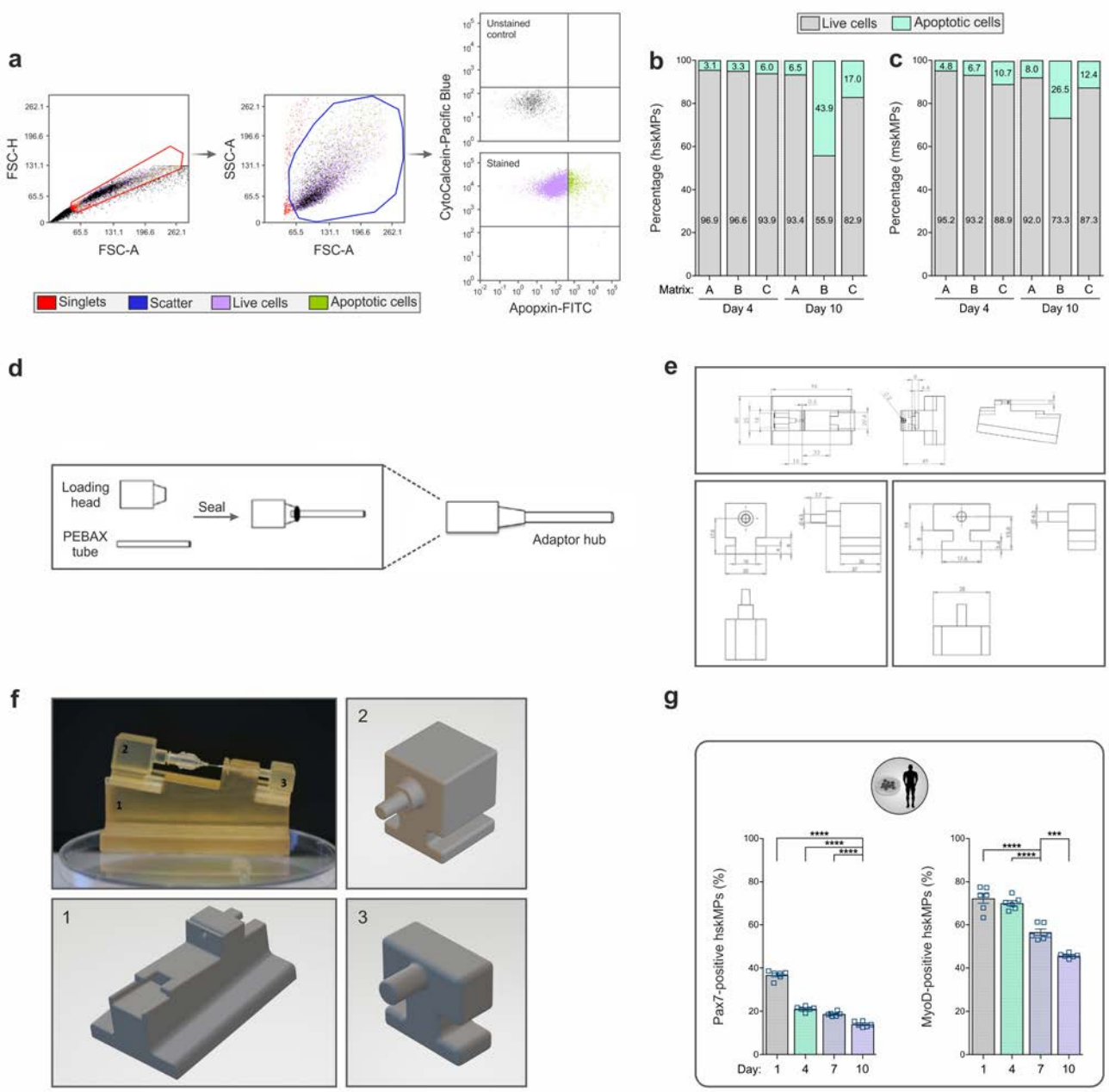
a
FSC-H
FSC-A
SSC-A
FSC-A
CytoCalcein-Pacific Blue
Apopxin-FITC
Unstained control
Stained
Singlets
Scatter
Live cells
Apoptotic cells
b
Live cells
Apoptotic cells
Percentage (hskMPs)
Matrix: A B C A B C
Day 4
Day 10
c
Percentage (mskMPs)
d
Loading head
PEBAX tube
Seal
Adaptor hub
e
f
g
Pax7-positive hskMPs (%)
MyoD-positive hskMPs (%)
Day: 1 4 7 10

Supplementary fig. 1 | a, Flow cytometry strategy used to identify live and apoptotic cells. CytoCalcein is sequestered in the cytoplasm of live cells, while apoptosis is measured by labeling of cell surface phosphatidylserine using Apopxin. **b**, Quantification of live and apoptotic human (hskMP) or mouse (mskMP) skeletal muscle progenitors embedded into different biomaterials and maintained in growth media for four or ten days. A=Growth factor reduced Matrigel, B=Hydrogel, C=MaxGel extracellular matrix. Values were obtained from pooled cells of n=6 replicates. **c**, Schematic outlining the construction of the adaptor hub used for mounting and loading of the capsules. **d**,**e**, Schematics and graphical representations of the parts of the 3D printed capsule cutting and sealing platform. The photograph in the upper left of (**f**) shows the assembled platform loaded with a capsule mounted to the adaptor hub. **g**, Quantification of Pax7 and MyoD positive hskMPs over a time course of ten days in 2D culture. Graphs represent means +/- s.e.m. n=6 replicates for each time-point. ****P<0.0001, ***P<0.001 by one–way ANOVA followed by Bonferroni post–test.

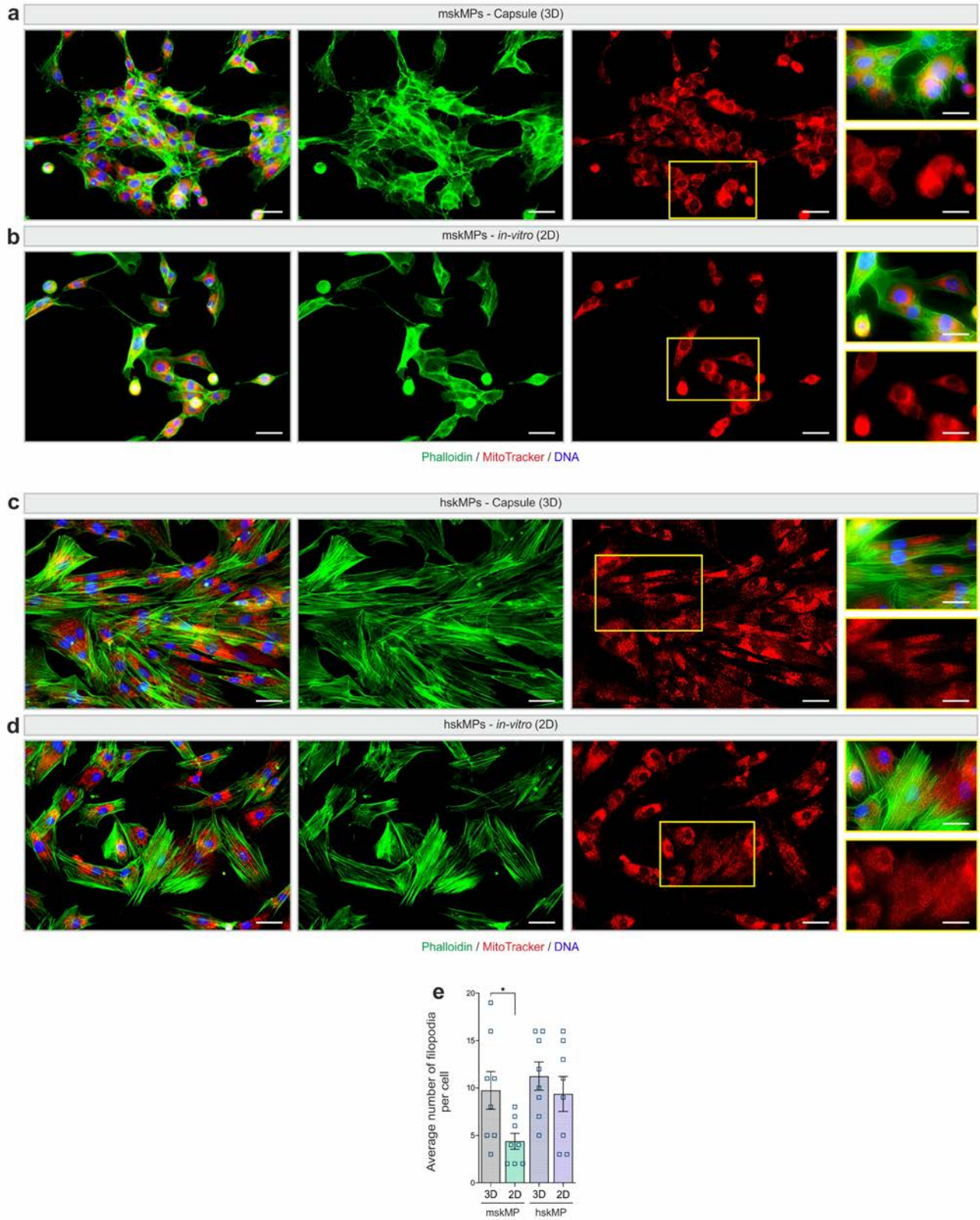
a
mskMPs - Capsule (3D)
b
mskMPs - in-vitro (2D)
Phalloidin / MitoTracker / DNA
c
hskMPs - Capsule (3D)
d
hskMPs - in-vitro (2D)
Phalloidin / MitoTracker / DNA
e
Average number of filopodia per cell
20
15
10
5
0
*
3D
2D
3D
2D
mskMP
hskMP

Supplementary fig. 2 | a-d, Representative phalloidin and MitoTracker stainings of hskMPs and mskMPs in cross sections of PES hollow fiber capsules and in 2D culture. Scale bars: 50 µm and 25 µm for inserts. **e**, Quantification of the number of filopodia in hskMPs and mskMPs in PES hollow fiber capsules and in 2D culture. n=8 replicates for each condition. Graphs represent means +/- s.e.m. *P<0.05 by one–way ANOVA followed by Bonferroni post–test.

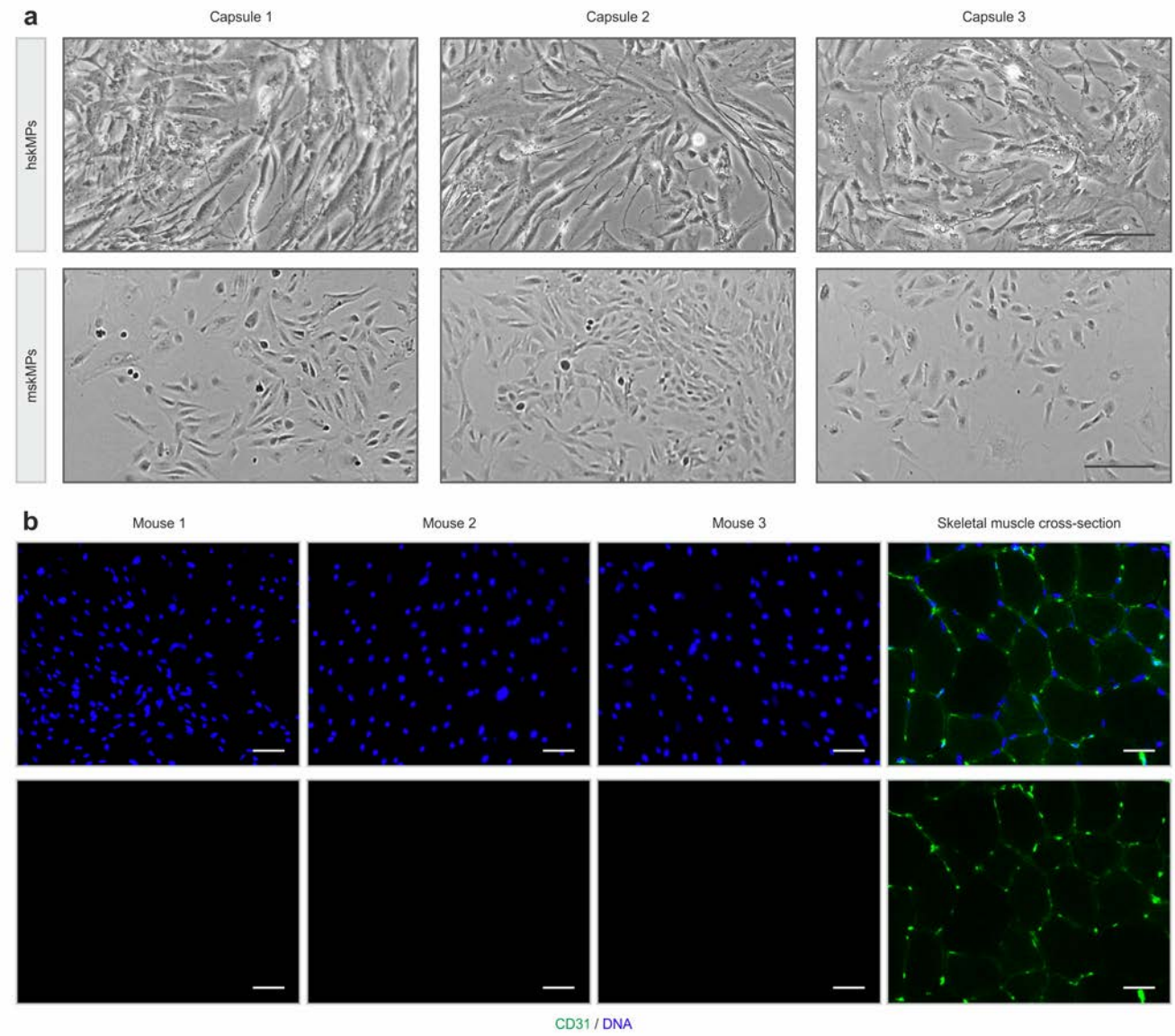

Supplementary fig. 3 | a, Representative bright field images of hskMPs and mskMPs in 2D culture after enzymatic liberation after encapsulation. Scale bars: 40 µm. **b**, Representative CD31 immunostainings of cross sections of PES hollow fiber capsules after ten days *in vivo*. Each image was taken capsules explanted from different animals. As a positive control CD31 staining of a mouse tibialis anterior muscle cross section is shown. Scale bars: 75 µm.

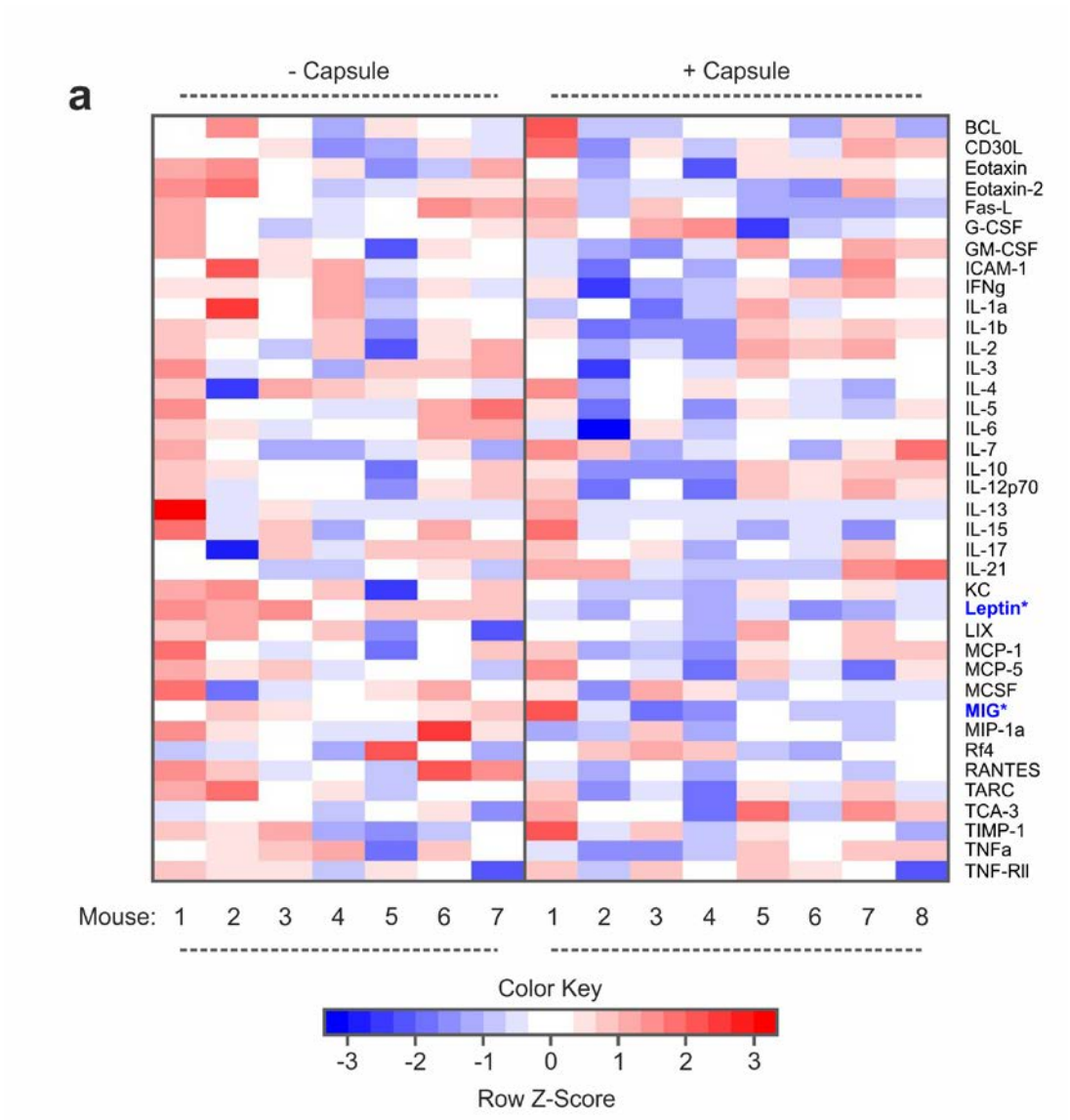

Supplementary fig. 4 | a, Multiplexed enzyme-linked immunosorbent assay (ELISA) array signal heatmaps for levels of inflammatory factors in serum of mice that underwent surgical implantation of PES hollow fiber capsules compared to untreated controls ten days after the procedure. n≥7 mice. Asterisks indicate factors changed with a p-value of ≤0.05 in a two-sample Wilcoxon test. TNF-RI and MIP-1g were excluded from the analysis since signals were outside of the detection range.

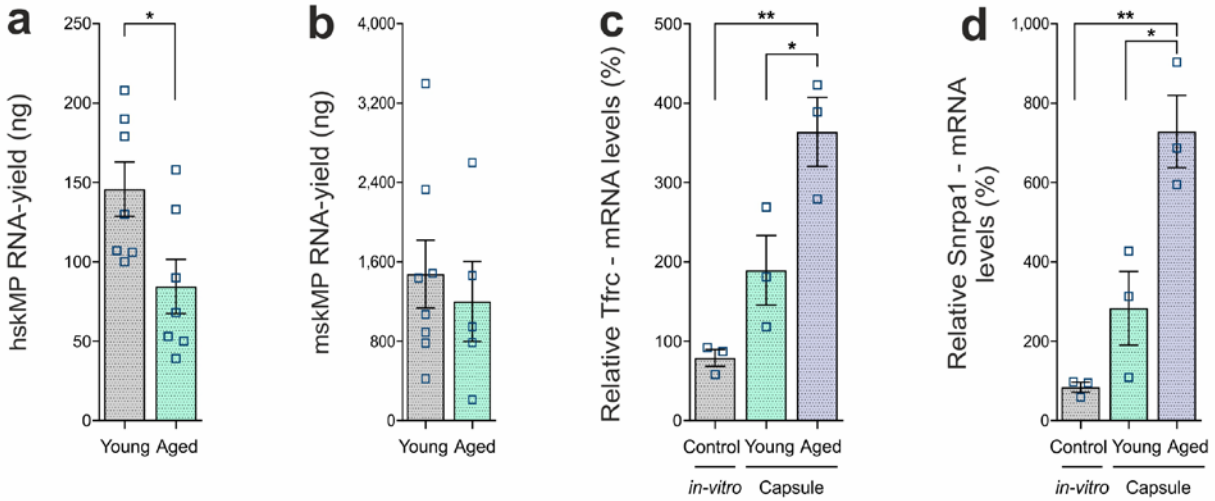

Supplementary fig. 5 | a,**b**, RNA yield from capsules containing hskMPs or mskMPs after ten days *in vivo* in young and aged mice. For each replicate two capsules from one mouse were pooled. Graphs represent means +/- s.e.m. Data is derived from capsules of n≥5 mice in each group. *P<0.05 by student's t–test. **c**,**d**, mRNA levels of the E2F target gene Tfrc and the Myc target Snrpa1 in hskMPs after ten days of encapsulation in young and aged mice. hskMPs in 2D culture were included as an expression control (*in-vitro*). Graphs represent means +/- s.e.m. n=3 mice (young and aged) or replicates (*in-vitro*) for each condition. **P<0.01, *P<0.05 by one–way ANOVA followed by Bonferroni post–test.

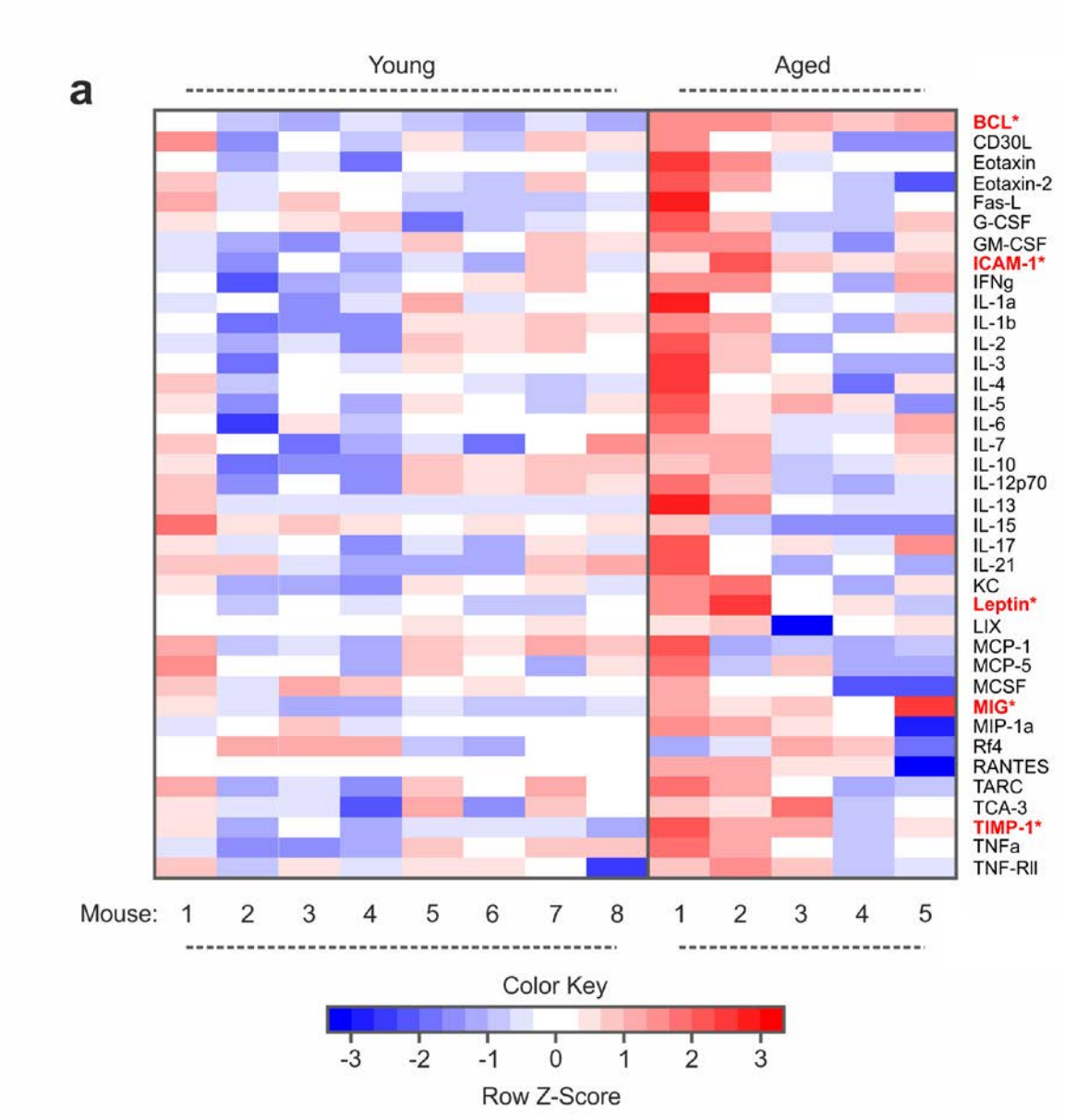

Supplementary fig. 6 | a, Multiplexed ELISA array heatmaps for levels of inflammatory factors in plasma of young and aged mice. n≥5 mice. Asterisks indicate factors changed with a p-value of ≤0.05 in a two-sample Wilcoxon test. TNF-RI and MIP-1g were excluded from the analysis since signals were outside of the detection range.

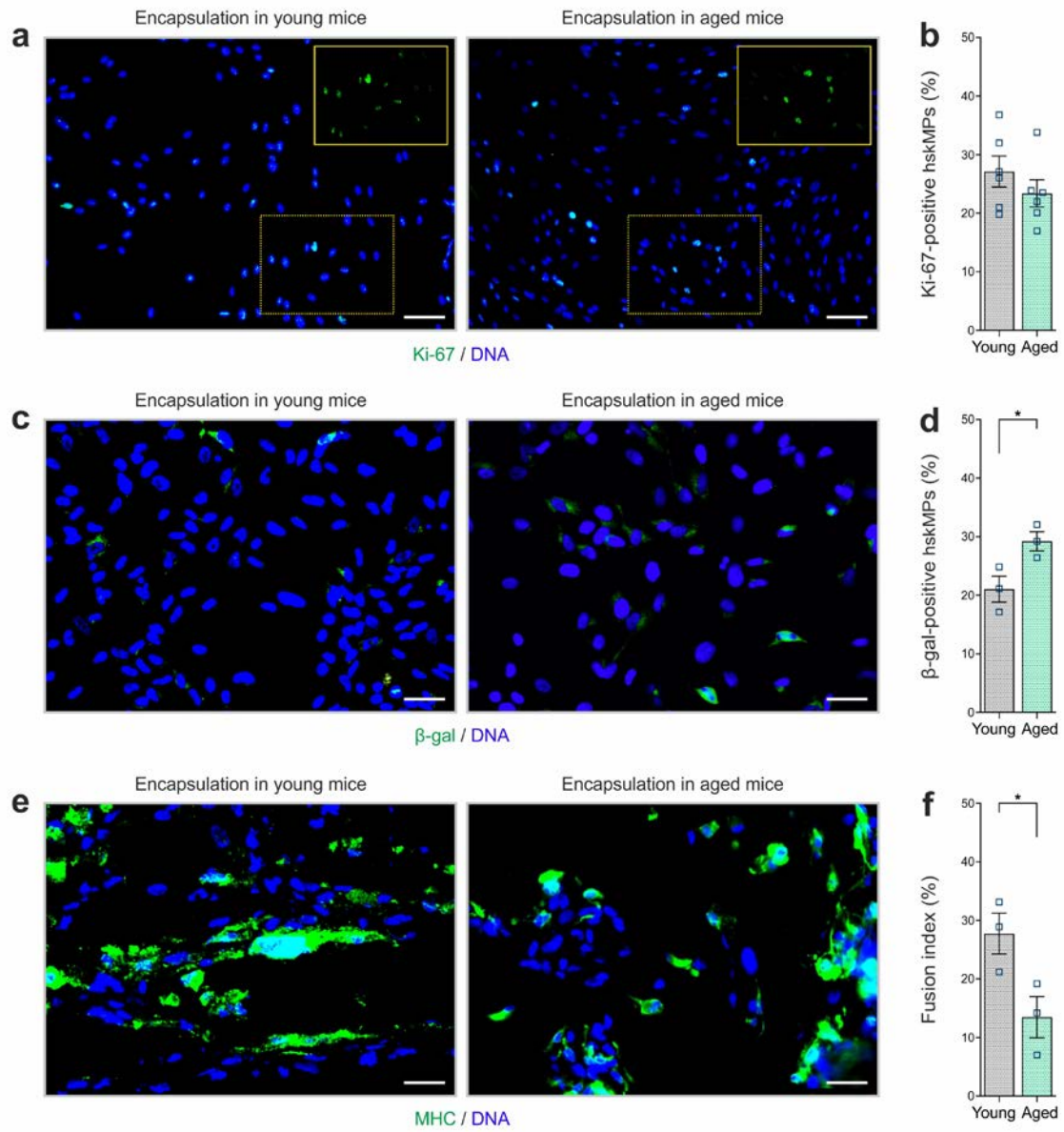

Supplementary fig. 7 | a,**b**, Representative Ki-67 immunostainings and quantification of cross sections of PES hollow fiber capsules containing hskMPs after ten days of exposure to the systemic environment in young and aged mice. **c**,**d**, Representative β-galactosidase (β-gal) immunostainings and quantification of cross sections of capsules containing hskMPs after ten days of exposure to the systemic environment in young and aged mice. **e**,**f**, Representative myosin heavy chain (MHC) immunostainings and quantification of the fusion index in cross sections of capsules containing hskMPs after ten days of exposure to the systemic environment in young and aged mice. Scale bars: 70 µm (a), 40 µm (b,c). Graphs represent means +/- s.e.m. Data is derived from n≥3 mice in each group. *P<0.05 by student's t–test.

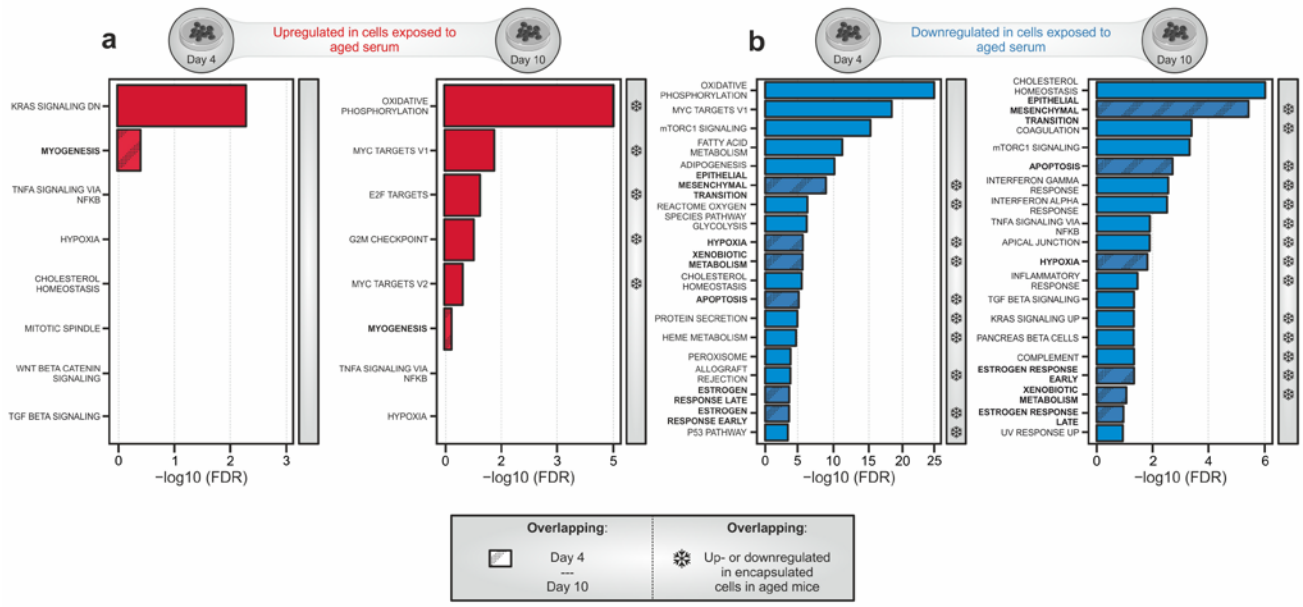

Supplementary fig. 8 | a, Gene set enrichment analysis (GSEA) of genes induced in hskMPs in 2D culture in the presence of aged human serum for four or ten days compared to the young condition. Gene sets that were also induced in encapsulated cells in aged mice (Fig. 4a) are marked by snowflakes. **b**, Gene set enrichment analysis (GSEA) of genes downregulated in hskMPs in 2D culture in the presence of aged human serum for four or ten days compared to the young condition. Gene sets that were also downregulated in encapsulated cells in aged mice (Fig. 4d) are marked by snowflakes. Samples and data are derived from hskMPs exposed to human serum from n=3 different young or aged donors. False discovery rate (FDR) = Adjusted p-value using Benjamini-Hochberg procedure.

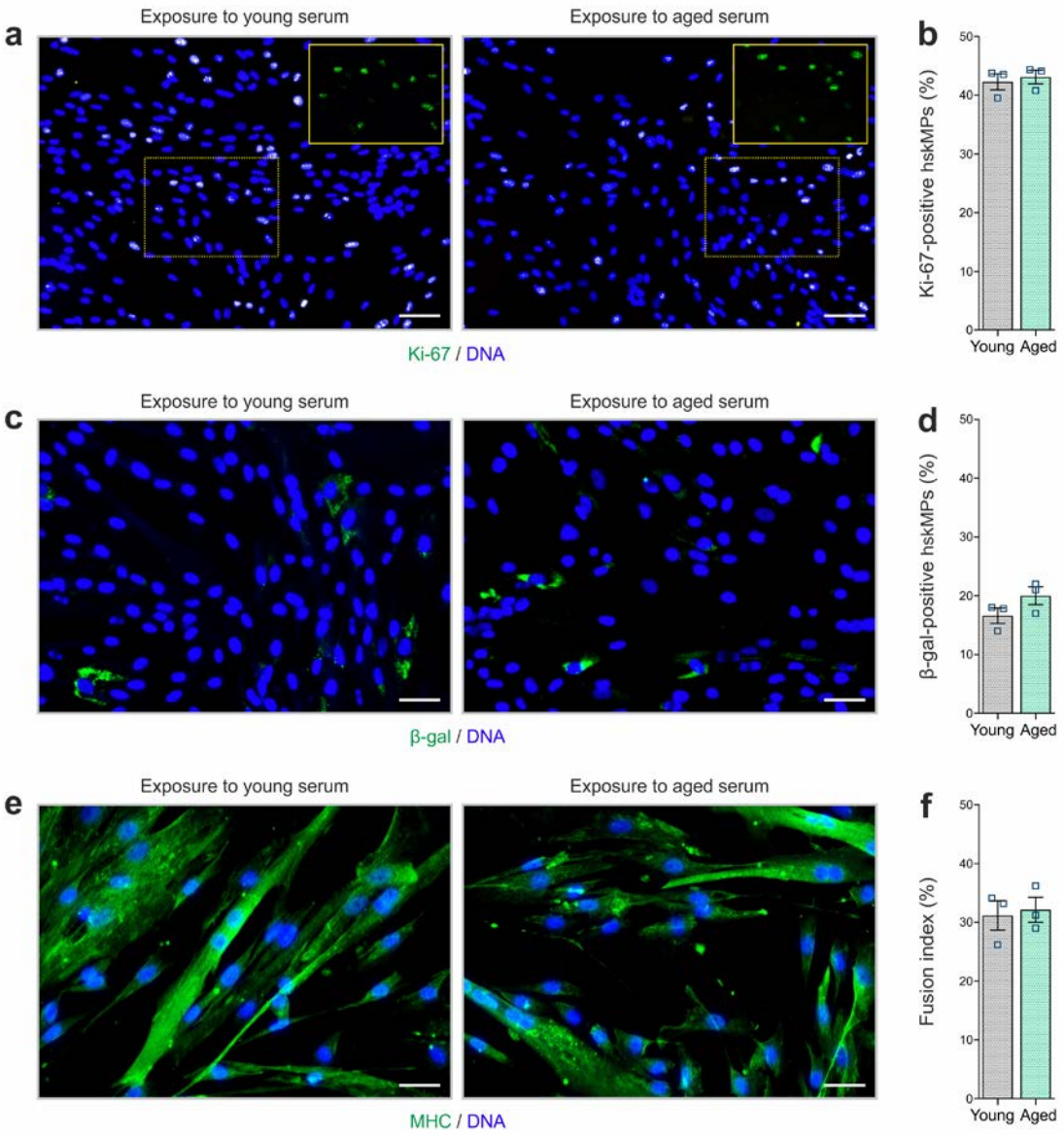

Supplementary fig. 9 | a,**b** Representative Ki-67 immunostainings and quantification of 2D cultured hskMPs exposed to young and aged human serum for 4 days. **c**,**d** Representative β-galactosidase (β-gal) immunostainings and quantification of 2D cultured hskMPs exposed to young and aged human serum for 4 days. **e**,**f** Representative myosin heavy chain (MHC) immunostainings and quantification of the fusion index of 2D hskMPs exposed to young and aged human serum under differentiation conditions for 4 days. Scale bars: 70 µm (a), 40 µm (b,c). Graphs represent means +/- s.e.m. Data is derived from n=3 replicates in young or aged serum. Significance was determined using student's t–test.

	- Capsule							+ Capsule							
Mouse	**1**	**2**	**3**	**4**	**5**	**6**	**7**	**1**	**2**	**3**	**4**	**5**	**6**	**7**	**8**
BLC	18.5	28.5	20.5	14.4	23.0	18.6	18.2	33.6	16.7	16.3	21.3	21.2	15.1	24.0	15.1
CD30L	11.2	9.4	13.9	1.1	5.4	13.3	8.2	35.2	3.1	13.2	6.7	15.2	6.9	21.8	18.8
Eotaxin	312.8	344.3	183.5	240.3	122.8	159.1	302.6	213.1	139.2	181.6	92.7	253.5	250.7	245.6	192.2
Eotaxin-2	165.7	212.9	96.7	63.6	80.9	107.4	118.4	125.8	66.0	71.5	72.6	57.8	52.9	153.6	78.4
Fas L	115.4	17.8	30.8	13.0	36.4	119.8	92.0	100.6	11.1	77.1	25.6	0.0	1.6	6.0	9.1
G-CSF	219.4	168.9	113.9	126.1	160.7	145.1	186.4	211.0	156.4	229.1	255.7	62.7	118.5	130.1	145.6
GM-CSF	26.2	20.3	21.3	19.2	9.9	21.7	20.6	16.1	12.6	12.0	16.2	27.0	19.2	27.2	25.3
ICAM-1	1873.4	2621.3	2061.8	2268.4	1723.5	1824.2	1947.8	1765.7	1440.2	1896.0	1588.8	1871.7	1597.9	2409.4	1874.0
IFNg	66.7	65.9	63.8	85.6	39.0	69.7	51.2	67.5	25.4	40.0	43.0	68.1	78.2	85.5	65.4
IL-1a	4.6	17.0	5.3	8.4	2.7	4.4	4.6	3.0	3.8	1.6	2.9	8.0	3.3	4.8	4.8
IL-1b	171.3	164.0	143.3	183.4	77.5	149.3	123.9	156.0	72.4	83.5	80.2	175.8	167.0	185.9	162.6
IL-2	116.4	91.6	77.9	116.6	57.5	106.1	122.5	88.0	74.8	84.9	69.0	123.7	114.0	121.2	97.2
IL-3	3.8	1.1	1.5	0.8	2.6	2.7	3.3	1.8	0.3	1.4	1.1	2.4	1.5	1.4	1.7
IL-4	2.2	0.0	2.8	2.3	1.9	1.6	1.1	3.6	0.8	1.7	1.9	1.5	1.1	0.8	1.3
IL-5	131.3	71.0	79.2	69.2	66.4	111.7	156.0	91.7	43.6	75.2	48.7	92.8	69.7	59.0	92.5
IL-6	23.6	19.5	11.3	16.4	14.4	25.3	25.8	11.9	3.0	17.9	9.7	17.0	14.7	14.6	15.9
IL-7	87.3	46.8	0.0	9.5	21.8	56.3	10.0	116.5	65.8	3.6	27.9	38.0	0.0	65.7	194.5
IL-10	324.7	307.3	261.2	272.0	119.3	262.4	309.6	287.5	139.5	147.3	142.0	340.5	292.4	316.5	323.1
IL-12p70	93.2	56.1	72.5	62.3	38.2	85.3	96.0	100.3	37.2	65.8	36.6	96.6	84.2	107.1	88.8
IL-13	171.3	6.2	18.5	4.8	4.5	0.0	0.0	31.4	0.0	0.9	6.4	0.0	0.0	3.1	0.0
IL-15	479.5	136.3	265.4	107.0	194.8	360.8	161.7	482.5	138.8	202.3	153.6	105.6	145.8	81.5	168.7
IL-17	2.1	0.1	4.0	1.2	3.6	3.5	4.1	3.6	1.7	2.7	0.9	2.0	1.2	3.6	1.8
IL-21	5.7	5.6	0.0	0.0	5.8	8.5	1.8	15.1	14.4	4.0	0.0	0.0	0.0	15.5	20.1
KC	4.6	4.8	3.6	4.4	2.0	3.3	4.4	3.7	2.9	2.9	2.7	3.9	3.5	3.9	3.2
Leptin	661.5	586.4	665.4	296.8	428.9	414.8	432.2	140.3	91.7	188.0	105.9	161.8	78.7	83.4	161.9
LIX	508.7	553.1	377.6	460.3	215.1	379.6	153.0	356.0	322.0	292.9	230.1	531.1	381.0	482.4	392.8
MCP-1	59.6	30.9	24.2	29.9	15.9	30.2	42.2	45.0	20.3	21.4	16.8	37.7	32.9	45.0	40.9
MCP-5	47.9	32.3	36.4	21.6	29.4	30.1	18.9	53.2	25.8	19.8	11.6	40.9	20.9	11.1	31.4
MCSF	9.6	0.7	1.9	3.4	4.1	7.2	2.6	4.3	0.8	6.1	3.7	1.5	3.1	2.0	1.7
MIG	41.0	49.3	45.0	40.9	42.3	43.7	46.2	67.0	35.5	25.7	28.1	36.9	31.8	32.8	40.9
MIP-1a	24.1	16.1	13.9	12.2	11.6	36.7	16.8	8.4	10.3	19.6	8.9	12.8	12.6	10.8	12.5
PF4	3066.6	3415.4	3692.6	3006.8	5273.3	3779.9	2905.3	3734.5	4274.5	4317.3	4222.6	3164.9	2978.8	3612.0	3644.5
RANTES	3.2	2.6	1.7	1.8	1.5	4.3	3.3	1.7	1.3	2.2	1.4	2.1	1.8	1.5	1.8
TARC	40.9	48.3	26.0	31.1	18.4	26.9	23.0	35.2	14.0	19.5	12.1	30.0	20.1	36.6	20.7
TCA-3	18.0	19.5	21.4	14.9	21.0	26.6	11.1	34.7	23.5	23.3	10.4	45.4	14.2	38.8	30.2
TIMP-1	597.3	575.2	638.2	442.1	431.9	456.9	512.9	721.0	479.6	587.1	472.9	563.8	544.4	555.8	445.5
TNFa	29.8	37.4	41.9	48.4	17.0	43.1	34.8	28.0	19.2	18.2	22.7	44.8	34.4	42.6	44.5
TNF RII	412.8	370.1	350.4	196.1	348.9	267.6	116.9	416.2	209.0	373.4	259.0	396.6	367.6	306.4	113.3

Supplementary table 1 | Multiplexed ELISA quantification of inflammatory factors in serum of mice that underwent surgical implantation of PES hollow fiber capsules compared to untreated controls ten days after the procedure. n≥7 mice. Each value represents averages in pg/ml from n=4 technical replicates for each factor. TNF-RI and MIP-1g were excluded from the analysis since signals were outside of the detection range.

Gene Set Name - Human	GST Pval	GST FDR
HALLMARK_MYC_TARGETS_V1	1.00E-04	0.005
HALLMARK_OXIDATIVE_PHOSPHORYLATION	2.00E-04	0.005
HALLMARK_E2F_TARGETS	0.0166	0.238
HALLMARK_FATTY_ACID_METABOLISM	0.0215	0.238
HALLMARK_PANCREAS_BETA_CELLS	0.0238	0.238
HALLMARK_ANGIOGENESIS	0.0648	0.506428571
HALLMARK_COAGULATION	0.0709	0.506428571
HALLMARK_KRAS_SIGNALING_UP	0.1885	1
HALLMARK_XENOBIOTIC_METABOLISM	0.1988	1
HALLMARK_ADIPOGENESIS	0.2427	1
HALLMARK_G2M_CHECKPOINT	0.2755	1
HALLMARK_REACTIVE_OXIGEN_SPECIES_PATHWAY	0.284	1
HALLMARK_SPERMATOGENESIS	0.3227	1
HALLMARK_ANDROGEN_RESPONSE	0.3554	1
HALLMARK_WNT_BETA_CATENIN_SIGNALING	0.3626	1
HALLMARK_PROTEIN_SECRETION	0.4046	1
HALLMARK_CHOLESTEROL_HOMEOSTASIS	0.5342	1
HALLMARK_MYC_TARGETS_V2	0.633	1
HALLMARK_BILE_ACID_METABOLISM	0.6826	1
HALLMARK_HEME_METABOLISM	0.7257	1
HALLMARK_TGF_BETA_SIGNALING	0.7263	1
HALLMARK_PEROXISOME	0.7279	1
HALLMARK_DNA_REPAIR	0.7765	1
HALLMARK_ALLOGRAFT_REJECTION	0.788	1
HALLMARK_MTORC1_SIGNALING	0.9169	1
HALLMARK_UV_RESPONSE_UP	0.9296	1
HALLMARK_APICAL_SURFACE	0.9408	1
HALLMARK_HEDGEHOG_SIGNALING	0.9426	1
HALLMARK_ESTROGEN_RESPONSE_LATE	0.9434	1
HALLMARK_IL2_STAT5_SIGNALING	0.961	1
HALLMARK_GLYCOLYSIS	0.963	1
HALLMARK_COMPLEMENT	0.964	1
HALLMARK_UV_RESPONSE_DN	0.9709	1
HALLMARK_APOPTOSIS	0.9756	1
HALLMARK_EPITHELIAL_MESENCHYMAL_TRANSITION	0.979	1
HALLMARK_INTERFERON_ALPHA_RESPONSE	0.9823	1
HALLMARK_UNFOLDED_PROTEIN_RESPONSE	0.9841	1
HALLMARK_APICAL_JUNCTION	0.9851	1
HALLMARK_NOTCH_SIGNALING	0.9871	1
HALLMARK_P53_PATHWAY	0.9898	1
HALLMARK_MITOTIC_SPINDLE	0.9913	1
HALLMARK_IL6_JAK_STAT3_SIGNALING	0.992	1
HALLMARK_PI3K_AKT_MTOR_SIGNALING	0.9961	1
HALLMARK_INTERFERON_GAMMA_RESPONSE	0.9976	1
HALLMARK_KRAS_SIGNALING_DN	0.9978	1
HALLMARK_HYPOXIA	0.9986	1
HALLMARK_INFLAMMATORY_RESPONSE	0.9988	1
HALLMARK_ESTROGEN_RESPONSE_EARLY	0.9996	1
HALLMARK_TNFA_SIGNALING_VIA_NFKB	0.9998	1
HALLMARK_MYOGENESIS	1	1

Supplementary table 2 | Gene sets increased with age in encapsulated hskMPs compared to the young control after ten days *in vivo*. Data are derived from capsules of n≥5 mice in each age group. GST Pval = Wilcoxon gene set test p- value. GST FDR = Adjusted p-value using the Benjamini-Hochberg procedure. GST FDR = Wilcoxon gene set test false discovery rate.

Gene Set Name - Mouse	GST Pval	GST FDR
HALLMARK_MITOTIC_SPINDLE	1.00E-04	0.00125
HALLMARK_G2M_CHECKPOINT	1.00E-04	0.00125
HALLMARK_E2F_TARGETS	1.00E-04	0.00125
HALLMARK_MYC_TARGETS_V1	1.00E-04	0.00125
HALLMARK_UV_RESPONSE_DN	0.0271	0.245833333
HALLMARK_MYC_TARGETS_V2	0.0295	0.245833333
HALLMARK_HEDGEHOG_SIGNALING	0.0512	0.365714286
HALLMARK_CHOLESTEROL_HOMEOSTASIS	0.1214	0.677777778
HALLMARK_KRAS_SIGNALING_DN	0.122	0.677777778
HALLMARK_NOTCH_SIGNALING	0.1655	0.8275
HALLMARK_TGF_BETA_SIGNALING	0.2272	1
HALLMARK_APICAL_JUNCTION	0.3936	1
HALLMARK_PI3K_AKT_MTOR_SIGNALING	0.4044	1
HALLMARK_ANDROGEN_RESPONSE	0.4386	1
HALLMARK_FATTY_ACID_METABOLISM	0.5445	1
HALLMARK_OXIDATIVE_PHOSPHORYLATION	0.5468	1
HALLMARK_MTORC1_SIGNALING	0.6076	1
HALLMARK_ESTROGEN_RESPONSE_LATE	0.653	1
HALLMARK_SPERMATOGENESIS	0.6719	1
HALLMARK_TNFA_SIGNALING_VIA_NFKB	0.712	1
HALLMARK_APICAL_SURFACE	0.7926	1
HALLMARK_INTERFERON_ALPHA_RESPONSE	0.7937	1
HALLMARK_UNFOLDED_PROTEIN_RESPONSE	0.8104	1
HALLMARK_APOPTOSIS	0.8208	1
HALLMARK_PEROXISOME	0.823	1
HALLMARK_HYPOXIA	0.8294	1
HALLMARK_WNT_BETA_CATENIN_SIGNALING	0.8509	1
HALLMARK_DNA_REPAIR	0.8616	1
HALLMARK_UV_RESPONSE_UP	0.8777	1
HALLMARK_ESTROGEN_RESPONSE_EARLY	0.8856	1
HALLMARK_GLYCOLYSIS	0.8878	1
HALLMARK_EPITHELIAL_MESENCHYMAL_TRANSITION	0.8937	1
HALLMARK_PROTEIN_SECRETION	0.9015	1
HALLMARK_MYOGENESIS	0.9268	1
HALLMARK_BILE_ACID_METABOLISM	0.9381	1
HALLMARK_PANCREAS_BETA_CELLS	0.9405	1
HALLMARK_ALLOGRAFT_REJECTION	0.9481	1
HALLMARK_HEME_METABOLISM	0.9549	1
HALLMARK_INTERFERON_GAMMA_RESPONSE	0.9629	1
HALLMARK_INFLAMMATORY_RESPONSE	0.9704	1
HALLMARK_ANGIOGENESIS	0.9902	1
HALLMARK_IL6_JAK_STAT3_SIGNALING	0.9955	1
HALLMARK_REACTIVE_OXIGEN_SPECIES_PATHWAY	0.9964	1
HALLMARK_ADIPOGENESIS	0.9986	1
HALLMARK_COMPLEMENT	0.9992	1
HALLMARK_P53_PATHWAY	0.9999	1
HALLMARK_XENOBIOTIC_METABOLISM	1	1
HALLMARK_COAGULATION	1	1
HALLMARK_IL2_STAT5_SIGNALING	1	1
HALLMARK_KRAS_SIGNALING_UP	1	1

Supplementary table 3 | Gene sets increased with age in encapsulated mskMPs compared to the young control after ten days *in vivo*. Data are derived from capsules of n≥5 mice in each age group. GST Pval = Wilcoxon gene set test p-value. GST FDR = Adjusted p-value using the Benjamini-Hochberg procedure.

Gene list Name: Human Myc	Entrez_Gene_ID	Pval
SNRPA1	6627	0.003392238
EEF1B2	1933	0.005434609
RAN	5901	0.006608012
HSPD1	3329	0.007032145
RPS3	6188	0.009164852
DHX15	1665	0.013753848
PSMA4	5685	0.013889751
EIF3B	8662	0.020952363
APEX1	328	0.024259783
PPM1G	5496	0.030717253
EIF4G2	1982	0.032850738
CLNS1A	1207	0.038547487
CNBP	7555	0.041247494
H2AFZ	3015	0.041308998
GOT2	2806	0.044374131
SFRS2	6427	0.050671179
PSMD14	10213	0.056216794
NCBP2	22916	0.056863238
AP3S1	1176	0.058218092
C1QBP	708	0.059635644
RPL34	6164	0.065106571
PSMA1	5682	0.067628383
SRM	6723	0.069279662
LSM7	51690	0.079526429
EIF4H	7458	0.089024704
HNRNPR	10236	0.091514993
ACP1	52	0.093385566
GLO1	2739	0.096041822
HDDC2	51020	0.10373487
ILF2	3608	0.105062374
KPNB1	3837	0.110552543
SF3B3	23450	0.116055116
TFDP1	7027	0.120165263
RRM1	6240	0.12146948
NME1	4830	0.124680277
RPS5	6193	0.133603961
PRDX3	10935	0.138578212
PSMA2	5683	0.145037331
RPLP0	6175	0.151014333
TYMS	7298	0.153238502
RUVBL2	10856	0.159409647
VDAC1	7416	0.165072978
PRDX4	10549	0.16886725
EXOSC7	23016	0.174912282
NOP16	51491	0.185175615
RPL18	6141	0.185269043
SMARCC1	6599	0.185794825
COPS5	10987	0.191437874
PWP1	11137	0.192517154
XPO1	7514	0.197505488
PABPC1	26986	0.208075705
XRCC6	2547	0.209376027
PA2G4	5036	0.221226783
LDHA	3939	0.225430805
MRPL23	6150	0.244494583
PHB	5245	0.252734546
CCT7	10574	0.258988772
RFC4	5984	0.268219724
PCBP1	5093	0.275406523
VBP1	7411	0.290212542

Gene list Name: Human Myc	Entrez_Gene_ID	Pval
PSMA6	5687	0.303152803
CDK4	1019	0.309228977
UBA2	10054	0.310913108
HNRNPU	3192	0.317074711
CCT3	7203	0.339467799
PHB2	11331	0.342385831
EPRS	2058	0.35703362
UBE2L3	7332	0.364117639
TOMM70A	9868	0.372195491
HNRPA2B1	3181	0.376637968
PSMB3	5691	0.387885477
PRPF31	26121	0.39110615
NOP56	10528	0.401195203
EIF1AX	1964	0.409281904
RPL14	9045	0.410832143
RANBP1	5902	0.413335163
GNB2L1	10399	0.414275317
RPS10	6204	0.43780544
SNRPD2	6633	0.446926748
EIF4A1	1973	0.459292469
DDX18	8886	0.482601512
MCM7	4176	0.489656126
SRPK1	6732	0.534856431
NHP2	55651	0.536197653
CBX3	11335	0.543034244
LSM2	57819	0.588783927
IMPDH2	3615	0.589423651
PRPS2	5634	0.589960777
HDAC2	3066	0.59311393
RPS2	6187	0.594295408
SNRPG	6637	0.600540544
SSBP1	6742	0.620666447
CUL1	8454	0.620751457
SNRPA	6626	0.620999589
POLD2	5425	0.623895233
MRPS18B	28973	0.628720883
FAM120A	23196	0.636059558
GSPT1	2935	0.647862269
PGK1	5230	0.649784957
CCNA2	890	0.655805663
RNPS1	10921	0.657031519
AIMP2	7965	0.668976235
HPRT1	3251	0.719650193
FBL	2091	0.719962808
HSP90AB1	3326	0.753094124
NCBP1	4686	0.757050736
USP1	7398	0.767226527
MCM5	4174	0.772826422
SLC25A3	5250	0.775933741
IFRD1	3475	0.786216915
ODC1	4953	0.789157714
SNRPB2	6629	0.790869565
TCP1	6950	0.817451206
CCT2	10576	0.826007656
TUFM	7284	0.832394346
SYNCRIP	10492	0.904366833
SFRS1	6426	0.960965928
RPL6	6128	0.971733909
HNRNPD	3184	0.977363883
PSMD1	5707	0.985781608

Supplementary table 4 | Significantly enriched Hallmark Myc V1 target genes when comparing encapsulated hskMPs in aged mice to the young control after ten days *in vivo*. Data are derived from capsules of n≥5 mice in each age group. P-value (Pval) <1%.

Gene list Name: Human E2F	Entrez_Gene_ID	Pval
RAN	5901	0.006608012
RPA2	6118	0.014860127
POLE4	56655	0.01802049
CKS1B	1163	0.024697221
CDKN1A	1026	0.032848419
H2AFZ	3015	0.041308998
TFRC	7037	0.044915398
SFRS2	6427	0.050671179
SLBP	7884	0.087256292
DCTPP1	79077	0.116609801
LSMD1	84316	0.117569831
NME1	4830	0.124680277
PHF5A	84844	0.130757893
KIF2C	11004	0.13211421
PRDX4	10549	0.16886725
XPO1	7514	0.197505488
XRCC6	2547	0.209376027
PA2G4	5036	0.221226783
HMGA1	3159	0.222380315
CSE1L	1434	0.281000763
MCM3	4172	0.281581876
NUP205	23165	0.294058659
CDK4	1019	0.309228977
NASP	4678	0.352631128
PLK4	10733	0.355090367
CBX5	23468	0.3614241
RAD21	5885	0.36235764
TUBG1	7283	0.369973582
UNG	7374	0.378476061
NOP56	10528	0.401195203
TUBB	203068	0.40819291
ILF3	3609	0.412356029
RANBP1	5902	0.413335163
LBR	3930	0.459788183
MCM7	4176	0.489656126
H2AFX	3014	0.492478323
CDCA8	55143	0.500398232
ZW10	9183	0.552227285
PTTG1	9232	0.570565713
BUB1B	701	0.575293758
RPA3	6119	0.6134248
POLD2	5425	0.623895233
GSPT1	2935	0.647862269
MTHFD2	10797	0.765228305
USP1	7398	0.767226527
MCM5	4174	0.772826422
CROP	51747	0.794736654
RFC1	5981	0.810546431
LOC146909	146909	0.813877648
DNMT1	1786	0.832302909
PDS5B	23047	0.845750177
MRE11A	4361	0.892357382
PRPS1	5631	0.904327377
SYNCRIP	10492	0.904366833
SNRPB	6628	0.912005837
SFRS1	6426	0.960965928
HNRNPD	3184	0.977363883
C6ORF167	253714	0.989129666
DDX39	10212	0.996693587

Supplementary table 5 | Significantly enriched Hallmark E2F target genes when comparing encapsulated hskMPs in aged mice to the young control after ten days *in vivo*. Data are derived from capsules of n≥5 mice in each age group. P-value (Pval) <1%.

	Young								Aged				
Mouse	**1**	**2**	**3**	**4**	**5**	**6**	**7**	**8**	**1**	**2**	**3**	**4**	**5**
BLC	33.6	16.7	16.3	21.3	21.2	15.1	24.0	15.1	95.8	112.4	75.9	69.4	81.6
CD30L	35.2	3.1	13.2	6.7	15.2	6.9	21.8	18.8	37.9	14.3	19.5	0.4	3.1
Eotaxin	213.1	139.2	181.6	92.7	253.5	250.7	245.6	192.2	703.0	454.6	192.3	233.9	271.6
Eotaxin-2	125.8	66.0	71.5	72.6	57.8	52.9	153.6	78.4	329.8	174.2	75.9	49.2	22.6
Fas L	100.6	11.1	77.1	25.6	0.0	1.6	6.0	9.1	943.1	22.5	27.0	0.0	20.7
G-CSF	211.0	156.4	229.1	255.7	62.7	118.5	130.1	145.6	518.0	241.5	112.8	108.0	240.6
GM-CSF	16.1	12.6	12.0	16.2	27.0	19.2	27.2	25.3	35.6	34.6	16.2	11.6	24.5
ICAM-1	1765.7	1440.2	1896.0	1588.8	1871.7	1597.9	2409.4	1874.0	2260.4	5278.9	2393.3	2234.2	2339.1
IFNg	67.5	25.4	40.0	43.0	68.1	78.2	85.5	65.4	117.5	119.0	55.4	36.4	100.7
IL-1a	3.0	3.8	1.6	2.9	8.0	3.3	4.8	4.8	25.4	3.7	3.1	3.4	2.8
IL-1b	156.0	72.4	83.5	80.2	175.8	167.0	185.9	162.6	248.9	232.1	143.7	94.0	195.3
IL-2	88.0	74.8	84.9	69.0	123.7	114.0	121.2	97.2	170.0	118.8	74.5	91.7	99.1
IL-3	1.8	0.3	1.4	1.1	2.4	1.5	1.4	1.7	8.8	2.8	1.9	0.7	0.7
IL-4	3.6	0.8	1.7	1.9	1.5	1.1	0.8	1.3	12.1	2.2	2.9	0.4	2.4
IL-5	91.7	43.6	75.2	48.7	92.8	69.7	59.0	92.5	175.4	88.6	122.1	88.4	42.2
IL-6	11.9	3.0	17.9	9.7	17.0	14.7	14.6	15.9	43.3	19.2	10.9	11.4	28.9
IL-7	116.5	65.8	3.6	27.9	38.0	0.0	65.7	194.5	161.4	146.0	45.5	75.2	113.8
IL-10	287.5	139.5	147.3	142.0	340.5	292.4	316.5	323.1	311.4	358.1	194.9	207.9	299.1
IL-12p70	100.3	37.2	65.8	36.6	96.6	84.2	107.1	88.8	147.1	109.6	49.2	47.1	54.4
IL-13	31.4	0.0	0.9	6.4	0.0	0.0	3.1	0.0	198.2	59.5	21.9	0.0	0.0
IL-15	482.5	138.8	202.3	153.6	105.6	145.8	81.5	168.7	228.9	61.3	0.0	0.0	0.0
IL-17	3.6	1.7	2.7	0.9	2.0	1.2	3.6	1.8	14.8	2.2	3.8	2.0	9.2
IL-21	15.1	14.4	4.0	0.0	0.0	0.0	15.5	20.1	45.4	8.3	2.4	7.0	0.0
KC	3.7	2.9	2.9	2.7	3.9	3.5	3.9	3.2	4.6	4.8	3.5	2.8	3.7
Leptin	140.3	91.7	188.0	105.9	161.8	78.7	83.4	161.9	687.3	1930.5	220.0	325.6	84.3
LIX	356.0	322.0	292.9	230.1	531.1	381.0	482.4	392.8	512.4	663.4	18.0	257.4	411.3
MCP-1	45.0	20.3	21.4	16.8	37.7	32.9	45.0	40.9	69.6	17.1	18.5	17.7	20.2
MCP-5	53.2	25.8	19.8	11.6	40.9	20.9	11.1	31.4	67.1	15.3	41.5	12.7	11.6
MCSF	4.3	0.8	6.1	3.7	1.5	3.1	2.0	1.7	9.4	0.9	2.0	0.1	0.1
MIG	67.0	35.5	25.7	28.1	36.9	31.8	32.8	40.9	92.5	70.8	77.6	52.1	201.7
MIP-1a	8.4	10.3	19.6	8.9	12.8	12.6	10.8	12.5	32.5	26.3	17.7	15.1	2.0
PF4	3734.5	4274.5	4317.3	4222.6	3164.9	2978.8	3612.0	3644.5	3049.0	3336.7	4330.0	4125.5	2772.5
RANTES	1.7	1.3	2.2	1.4	2.1	1.8	1.5	1.8	5.7	5.2	3.1	2.5	0.1
TARC	35.2	14.0	19.5	12.1	30.0	20.1	36.6	20.7	44.1	34.6	21.4	13.3	16.0
TCA-3	34.7	23.5	23.3	10.4	45.4	14.2	38.8	30.2	40.2	34.9	63.9	18.7	25.9
TIMP-1	721.0	479.6	587.1	472.9	563.8	544.4	555.8	445.5	1055.8	851.2	830.4	505.2	694.6
TNFa	28.0	19.2	18.2	22.7	44.8	34.4	42.6	44.5	64.1	50.0	29.7	23.1	35.7
TNF RII	416.2	209.0	373.4	259.0	396.6	367.6	306.4	113.3	439.8	542.5	401.2	225.7	248.6

Supplementary table 6 | Multiplexed ELISA array quantification of levels of inflammatory factors in plasma of mice young and aged mice. n≥5 mice. Each value represents averages in pg/ml from n=4 technical replicates for each factor. TNF-RI and MIP-1g were excluded from the analysis since signals were outside of the detection range.

Gene Set Name - Human	GST Pval	GST FDR
HALLMARK_TNFA_SIGNALING_VIA_NFKB	1.00E-04	0.0025
HALLMARK_MYOGENESIS	1.00E-04	0.0025
HALLMARK_ESTROGEN_RESPONSE_EARLY	4.00E-04	0.006666667
HALLMARK_INFLAMMATORY_RESPONSE	0.0012	0.015
HALLMARK_KRAS_SIGNALING_DN	0.0022	0.018571429
HALLMARK_HYPOXIA	0.0026	0.018571429
HALLMARK_INTERFERON_GAMMA_RESPONSE	0.0026	0.018571429
HALLMARK_PI3K_AKT_MTOR_SIGNALING	0.004	0.025
HALLMARK_IL6_JAK_STAT3_SIGNALING	0.0067	0.037222222
HALLMARK_MITOTIC_SPINDLE	0.0082	0.041
HALLMARK_P53_PATHWAY	0.0112	0.04875
HALLMARK_NOTCH_SIGNALING	0.0117	0.04875
HALLMARK_APICAL_JUNCTION	0.0139	0.053461538
HALLMARK_INTERFERON_ALPHA_RESPONSE	0.0159	0.055
HALLMARK_UNFOLDED_PROTEIN_RESPONSE	0.0165	0.055
HALLMARK_EPITHELIAL_MESENCHYMAL_TRANSITION	0.022	0.06875
HALLMARK_APOPTOSIS	0.0246	0.072352941
HALLMARK_UV_RESPONSE_DN	0.0331	0.085714286
HALLMARK_IL2_STAT5_SIGNALING	0.0352	0.085714286
HALLMARK_COMPLEMENT	0.0353	0.085714286
HALLMARK_GLYCOLYSIS	0.036	0.085714286
HALLMARK_ESTROGEN_RESPONSE_LATE	0.0493	0.112045455
HALLMARK_HEDGEHOG_SIGNALING	0.0537	0.11673913
HALLMARK_APICAL_SURFACE	0.0593	0.123541667
HALLMARK_UV_RESPONSE_UP	0.0726	0.1452
HALLMARK_MTORC1_SIGNALING	0.0827	0.159038462
HALLMARK_ALLOGRAFT_REJECTION	0.2044	0.378518519
HALLMARK_DNA_REPAIR	0.225	0.401785714
HALLMARK_HEME_METABOLISM	0.2687	0.449193548
HALLMARK_PEROXISOME	0.2711	0.449193548
HALLMARK_TGF_BETA_SIGNALING	0.2785	0.449193548
HALLMARK_BILE_ACID_METABOLISM	0.3176	0.49625
HALLMARK_MYC_TARGETS_V2	0.376	0.56969697
HALLMARK_CHOLESTEROL_HOMEOSTASIS	0.4723	0.694558824
HALLMARK_PROTEIN_SECRETION	0.5884	0.840571429
HALLMARK_ANDROGEN_RESPONSE	0.6312	0.857837838
HALLMARK_WNT_BETA_CATENIN_SIGNALING	0.6348	0.857837838
HALLMARK_SPERMATOGENESIS	0.6707	0.8825
HALLMARK_REACTIVE_OXIGEN_SPECIES_PATHWAY	0.7166	0.896875
HALLMARK_G2M_CHECKPOINT	0.7175	0.896875
HALLMARK_ADIPOGENESIS	0.7542	0.919756098
HALLMARK_XENOBIOTIC_METABOLISM	0.8072	0.952790698
HALLMARK_KRAS_SIGNALING_UP	0.8194	0.952790698
HALLMARK_COAGULATION	0.9334	1
HALLMARK_ANGIOGENESIS	0.9352	1
HALLMARK_PANCREAS_BETA_CELLS	0.9707	1
HALLMARK_FATTY_ACID_METABOLISM	0.9777	1
HALLMARK_E2F_TARGETS	0.9846	1
HALLMARK_OXIDATIVE_PHOSPHORYLATION	0.9996	1
HALLMARK_MYC_TARGETS_V1	1	1

Supplementary table 7 | Gene sets decreased with age in encapsulated hskMPs compared to the young control after ten days *in vivo*. Data are derived from capsules of n≥5 mice in each age group. GST Pval = Wilcoxon gene set test p-value. GST FDR = Adjusted p-value using the Benjamini-Hochberg procedure.

Gene Set Name - Mouse	GST Pval	GST FDR
HALLMARK_XENOBIOTIC_METABOLISM	1.00E-04	0.001
HALLMARK_P53_PATHWAY	1.00E-04	0.001
HALLMARK_COAGULATION	1.00E-04	0.001
HALLMARK_IL2_STAT5_SIGNALING	1.00E-04	0.001
HALLMARK_KRAS_SIGNALING_UP	1.00E-04	0.001
HALLMARK_COMPLEMENT	8.00E-04	0.006666667
HALLMARK_ADIPOGENESIS	0.0018	0.012857143
HALLMARK_IL6_JAK_STAT3_SIGNALING	0.0036	0.0225
HALLMARK_REACTIVE_OXIGEN_SPECIES_PATHWAY	0.0043	0.023888889
HALLMARK_ANGIOGENESIS	0.0089	0.0445
HALLMARK_INFLAMMATORY_RESPONSE	0.0296	0.134545455
HALLMARK_INTERFERON_GAMMA_RESPONSE	0.0348	0.145
HALLMARK_HEME_METABOLISM	0.0391	0.150384615
HALLMARK_ALLOGRAFT_REJECTION	0.0561	0.198823529
HALLMARK_PANCREAS_BETA_CELLS	0.0606	0.198823529
HALLMARK_BILE_ACID_METABOLISM	0.0648	0.198823529
HALLMARK_MYOGENESIS	0.0676	0.198823529
HALLMARK_PROTEIN_SECRETION	0.0918	0.255
HALLMARK_EPITHELIAL_MESENCHYMAL_TRANSITION	0.1071	0.268809524
HALLMARK_ESTROGEN_RESPONSE_EARLY	0.1125	0.268809524
HALLMARK_GLYCOLYSIS	0.1129	0.268809524
HALLMARK_UV_RESPONSE_UP	0.1237	0.281136364
HALLMARK_DNA_REPAIR	0.1388	0.30173913
HALLMARK_WNT_BETA_CATENIN_SIGNALING	0.1468	0.305833333
HALLMARK_HYPOXIA	0.1736	0.334038462
HALLMARK_PEROXISOME	0.1737	0.334038462
HALLMARK_APOPTOSIS	0.183	0.33625
HALLMARK_UNFOLDED_PROTEIN_RESPONSE	0.1883	0.33625
HALLMARK_INTERFERON_ALPHA_RESPONSE	0.2077	0.3485
HALLMARK_APICAL_SURFACE	0.2091	0.3485
HALLMARK_TNFA_SIGNALING_VIA_NFKB	0.2938	0.473870968
HALLMARK_SPERMATOGENESIS	0.3287	0.51359375
HALLMARK_ESTROGEN_RESPONSE_LATE	0.3518	0.533030303
HALLMARK_MTORC1_SIGNALING	0.3919	0.576323529
HALLMARK_FATTY_ACID_METABOLISM	0.4534	0.640555556
HALLMARK_OXIDATIVE_PHOSPHORYLATION	0.4612	0.640555556
HALLMARK_ANDROGEN_RESPONSE	0.5669	0.766081081
HALLMARK_PI3K_AKT_MTOR_SIGNALING	0.5979	0.768333333
HALLMARK_APICAL_JUNCTION	0.5993	0.768333333
HALLMARK_TGF_BETA_SIGNALING	0.7692	0.9615
HALLMARK_NOTCH_SIGNALING	0.8402	1
HALLMARK_CHOLESTEROL_HOMEOSTASIS	0.873	1
HALLMARK_KRAS_SIGNALING_DN	0.8786	1
HALLMARK_HEDGEHOG_SIGNALING	0.9466	1
HALLMARK_UV_RESPONSE_DN	0.9712	1
HALLMARK_MYC_TARGETS_V2	0.9741	1
HALLMARK_MITOTIC_SPINDLE	1	1
HALLMARK_G2M_CHECKPOINT	1	1
HALLMARK_E2F_TARGETS	1	1
HALLMARK_MYC_TARGETS_V1	1	1

Supplementary table 8 | Gene sets decreased with age in encapsulated mskMPs compared to the young control after ten days *in vivo*. Data are derived from capsules of n≥5 mice in each age group. GST Pval = Wilcoxon gene set test p-value. GST FDR = Adjusted p-value using the Benjamini-Hochberg procedure.

Gene Set Name - Freshly Isolated MPs	GST Pval	GST FDR
HALLMARK_TNFA_SIGNALING_VIA_NFKB	1.00E-04	0.000714286
HALLMARK_INTERFERON_ALPHA_RESPONSE	1.00E-04	0.000714286
HALLMARK_INTERFERON_GAMMA_RESPONSE	1.00E-04	0.000714286
HALLMARK_E2F_TARGETS	1.00E-04	0.000714286
HALLMARK_XENOBIOTIC_METABOLISM	1.00E-04	0.000714286
HALLMARK_FATTY_ACID_METABOLISM	1.00E-04	0.000714286
HALLMARK_ALLOGRAFT_REJECTION	1.00E-04	0.000714286
HALLMARK_MTORC1_SIGNALING	2.00E-04	0.001111111
HALLMARK_MYC_TARGETS_V2	2.00E-04	0.001111111
HALLMARK_OXIDATIVE_PHOSPHORYLATION	4.00E-04	0.002
HALLMARK_G2M_CHECKPOINT	8.00E-04	0.003636364
HALLMARK_IL6_JAK_STAT3_SIGNALING	0.0028	0.011153846
HALLMARK_INFLAMMATORY_RESPONSE	0.0029	0.011153846
HALLMARK_REACTIVE_OXIGEN_SPECIES_PATHWAY	0.0039	0.013928571
HALLMARK_MYC_TARGETS_V1	0.0047	0.015666667
HALLMARK_APOPTOSIS	0.0074	0.023125
HALLMARK_BILE_ACID_METABOLISM	0.0194	0.057058824
HALLMARK_KRAS_SIGNALING_UP	0.0265	0.073611111
HALLMARK_COMPLEMENT	0.0371	0.097631579
HALLMARK_DNA_REPAIR	0.0452	0.113
HALLMARK_PEROXISOME	0.0858	0.204285714
HALLMARK_SPERMATOGENESIS	0.1062	0.241363636
HALLMARK_GLYCOLYSIS	0.1574	0.342173913
HALLMARK_APICAL_SURFACE	0.2034	0.42375
HALLMARK_ESTROGEN_RESPONSE_LATE	0.2152	0.4304
HALLMARK_IL2_STAT5_SIGNALING	0.2275	0.4375
HALLMARK_ADIPOGENESIS	0.2721	0.503888889
HALLMARK_CHOLESTEROL_HOMEOSTASIS	0.2845	0.508035714
HALLMARK_UNFOLDED_PROTEIN_RESPONSE	0.326	0.562068966
HALLMARK_PANCREAS_BETA_CELLS	0.39	0.65
HALLMARK_HEME_METABOLISM	0.4151	0.65890625
HALLMARK_COAGULATION	0.4217	0.65890625
HALLMARK_P53_PATHWAY	0.4672	0.707878788
HALLMARK_HYPOXIA	0.4937	0.726029412
HALLMARK_ANDROGEN_RESPONSE	0.556	0.794285714
HALLMARK_PI3K_AKT_MTOR_SIGNALING	0.5926	0.823055556
HALLMARK_UV_RESPONSE_UP	0.7824	1
HALLMARK_ESTROGEN_RESPONSE_EARLY	0.8029	1
HALLMARK_WNT_BETA_CATENIN_SIGNALING	0.8277	1
HALLMARK_PROTEIN_SECRETION	0.841	1
HALLMARK_TGF_BETA_SIGNALING	0.9167	1
HALLMARK_NOTCH_SIGNALING	0.9188	1
HALLMARK_HEDGEHOG_SIGNALING	0.9471	1
HALLMARK_MITOTIC_SPINDLE	0.9955	1
HALLMARK_KRAS_SIGNALING_DN	0.9984	1
HALLMARK_MYOGENESIS	0.9994	1
HALLMARK_APICAL_JUNCTION	0.9996	1
HALLMARK_UV_RESPONSE_DN	0.9999	1
HALLMARK_EPITHELIAL_MESENCHYMAL_TRANSITION	1	1
HALLMARK_ANGIOGENESIS	1	1

Supplementary table 9 | Gene sets increased with age in niche resident freshly isolated mouse muscle stem cells compared to the young control. Data from n=8 young or aged mice. GST Pval = Wilcoxon gene set test p-value. GST FDR = Adjusted p-value using the Benjamini-Hochberg procedure.

Gene Set Name - Freshly Isolated MPs	GST Pval	GST FDR
HALLMARK_EPITHELIAL_MESENCHYMAL_TRANSITION	1.00E-04	0.001666667
HALLMARK_UV_RESPONSE_DN	1.00E-04	0.001666667
HALLMARK_ANGIOGENESIS	1.00E-04	0.001666667
HALLMARK_MYOGENESIS	2.00E-04	0.0025
HALLMARK_APICAL_JUNCTION	4.00E-04	0.004
HALLMARK_KRAS_SIGNALING_DN	0.0019	0.015833333
HALLMARK_MITOTIC_SPINDLE	0.0055	0.039285714
HALLMARK_HEDGEHOG_SIGNALING	0.0509	0.318125
HALLMARK_NOTCH_SIGNALING	0.0785	0.435
HALLMARK_TGF_BETA_SIGNALING	0.087	0.435
HALLMARK_PROTEIN_SECRETION	0.1603	0.728636364
HALLMARK_WNT_BETA_CATENIN_SIGNALING	0.1808	0.739615385
HALLMARK_ESTROGEN_RESPONSE_EARLY	0.1923	0.739615385
HALLMARK_UV_RESPONSE_UP	0.2166	0.773571429
HALLMARK_PI3K_AKT_MTOR_SIGNALING	0.3975	1
HALLMARK_ANDROGEN_RESPONSE	0.4511	1
HALLMARK_HYPOXIA	0.5136	1
HALLMARK_P53_PATHWAY	0.5311	1
HALLMARK_COAGULATION	0.585	1
HALLMARK_HEME_METABOLISM	0.5856	1
HALLMARK_PANCREAS_BETA_CELLS	0.6043	1
HALLMARK_UNFOLDED_PROTEIN_RESPONSE	0.667	1
HALLMARK_CHOLESTEROL_HOMEOSTASIS	0.7074	1
HALLMARK_ADIPOGENESIS	0.7445	1
HALLMARK_IL2_STAT5_SIGNALING	0.768	1
HALLMARK_ESTROGEN_RESPONSE_LATE	0.7814	1
HALLMARK_APICAL_SURFACE	0.8004	1
HALLMARK_GLYCOLYSIS	0.8457	1
HALLMARK_SPERMATOGENESIS	0.8918	1
HALLMARK_PEROXISOME	0.9184	1
HALLMARK_DNA_REPAIR	0.9581	1
HALLMARK_COMPLEMENT	0.9625	1
HALLMARK_KRAS_SIGNALING_UP	0.9756	1
HALLMARK_BILE_ACID_METABOLISM	0.9823	1
HALLMARK_APOPTOSIS	0.9911	1
HALLMARK_REACTIVE_OXIGEN_SPECIES_PATHWAY	0.9948	1
HALLMARK_MYC_TARGETS_V1	0.9957	1
HALLMARK_IL6_JAK_STAT3_SIGNALING	0.9977	1
HALLMARK_INFLAMMATORY_RESPONSE	0.9982	1
HALLMARK_MTORC1_SIGNALING	0.9998	1
HALLMARK_G2M_CHECKPOINT	0.9999	1
HALLMARK_FATTY_ACID_METABOLISM	0.9999	1
HALLMARK_TNFA_SIGNALING_VIA_NFKB	1	1
HALLMARK_INTERFERON_ALPHA_RESPONSE	1	1
HALLMARK_INTERFERON_GAMMA_RESPONSE	1	1
HALLMARK_E2F_TARGETS	1	1
HALLMARK_MYC_TARGETS_V2	1	1
HALLMARK_XENOBIOTIC_METABOLISM	1	1
HALLMARK_OXIDATIVE_PHOSPHORYLATION	1	1
HALLMARK_ALLOGRAFT_REJECTION	1	1

Supplementary table 10 | Gene sets decreased with age in niche resident freshly isolated mouse muscle stem cells compared to the young control. Data from n=3 young or aged mice. GST Pval = Wilcoxon gene set test p-value. GST FDR = Adjusted p-value using the Benjamini-Hochberg procedure.

Gene Set Name: Human - D4 - *in-vitro*	**GST_Pval**	**GST_FDR**
HALLMARK_KRAS_SIGNALING_DN	7.38184E-05	0.003690921
HALLMARK_MYOGENESIS	0.016547233	0.413680814
HALLMARK_MITOTIC_SPINDLE	0.092710962	1
HALLMARK_WNT_BETA_CATENIN_SIGNALING	0.127484809	1
HALLMARK_SPERMATOGENESIS	0.155043207	1
HALLMARK_HEDGEHOG_SIGNALING	0.308988817	1
HALLMARK_KRAS_SIGNALING_UP	0.489306906	1
HALLMARK_UV_RESPONSE_DN	0.502201637	1
HALLMARK_NOTCH_SIGNALING	0.523833904	1
HALLMARK_G2M_CHECKPOINT	0.629324403	1
HALLMARK_APICAL_SURFACE	0.754826941	1
HALLMARK_E2F_TARGETS	0.780390542	1
HALLMARK_ANGIOGENESIS	0.866321537	1
HALLMARK_INTERFERON_ALPHA_RESPONSE	0.909711872	1
HALLMARK_INFLAMMATORY_RESPONSE	0.918050427	1
HALLMARK_APICAL_JUNCTION	0.919415481	1
HALLMARK_PANCREAS_BETA_CELLS	0.940161163	1
HALLMARK_IL2_STAT5_SIGNALING	0.960055152	1
HALLMARK_TNFA_SIGNALING_VIA_NFKB	0.966177046	1
HALLMARK_INTERFERON_GAMMA_RESPONSE	0.967155442	1
HALLMARK_TGF_BETA_SIGNALING	0.972137076	1
HALLMARK_IL6_JAK_STAT3_SIGNALING	0.983257911	1
HALLMARK_MYC_TARGETS_V2	0.988243344	1
HALLMARK_BILE_ACID_METABOLISM	0.993171096	1
HALLMARK_COMPLEMENT	0.995493526	1
HALLMARK_DNA_REPAIR	0.996835177	1
HALLMARK_UNFOLDED_PROTEIN_RESPONSE	0.996925414	1
HALLMARK_UV_RESPONSE_UP	0.998857485	1
HALLMARK_ANDROGEN_RESPONSE	0.999000297	1
HALLMARK_COAGULATION	0.999724498	1
HALLMARK_PI3K_AKT_MTOR_SIGNALING	0.999749468	1
HALLMARK_P53_PATHWAY	0.99977587	1
HALLMARK_ESTROGEN_RESPONSE_EARLY	0.999855771	1
HALLMARK_ESTROGEN_RESPONSE_LATE	0.999880179	1
HALLMARK_ALLOGRAFT_REJECTION	0.999921122	1
HALLMARK_PEROXISOME	0.99993053	1
HALLMARK_HEME_METABOLISM	0.999989611	1
HALLMARK_PROTEIN_SECRETION	0.999993718	1
HALLMARK_APOPTOSIS	0.999996336	1
HALLMARK_CHOLESTEROL_HOMEOSTASIS	0.999998683	1
HALLMARK_XENOBIOTIC_METABOLISM	0.999999212	1
HALLMARK_HYPOXIA	0.999999372	1
HALLMARK_GLYCOLYSIS	0.999999863	1
HALLMARK_REACTIVE_OXIGEN_SPECIES_PATHWAY	0.999999898	1
HALLMARK_EPITHELIAL_MESENCHYMAL_TRANSITION	1	1
HALLMARK_ADIPOGENESIS	1	1
HALLMARK_FATTY_ACID_METABOLISM	1	1
HALLMARK_MTORC1_SIGNALING	1	1
HALLMARK_MYC_TARGETS_V1	1	1
HALLMARK_OXIDATIVE_PHOSPHORYLATION	1	1

Supplementary table 11 | Gene sets increased after four days in 2D hskMP culture exposed to aged human serum compared to the young human serum. GST Pval = Wilcoxon gene set test p-value. Data are derived from hskMPs exposed to human serum from n=3 different young or aged donors. GST FDR = Adjusted p-value using the Benjamini-Hochberg procedure.

Gene Set Name: Human - D10 - *in-vitro*	**GST_Pval**	**GST_FDR**
HALLMARK_OXIDATIVE_PHOSPHORYLATION	2.36115E-07	1.18058E-05
HALLMARK_MYC_TARGETS_V1	0.000955568	0.0238892
HALLMARK_E2F_TARGETS	0.003459696	0.057661598
HALLMARK_G2M_CHECKPOINT	0.00849323	0.106165371
HALLMARK_MYC_TARGETS_V2	0.029563729	0.295637295
HALLMARK_MYOGENESIS	0.074208319	0.618402659
HALLMARK_MITOTIC_SPINDLE	0.193517125	0.999999997
HALLMARK_SPERMATOGENESIS	0.237153025	0.999999997
HALLMARK_ADIPOGENESIS	0.246304701	0.999999997
HALLMARK_DNA_REPAIR	0.307501786	0.999999997
HALLMARK_WNT_BETA_CATENIN_SIGNALING	0.318443285	0.999999997
HALLMARK_NOTCH_SIGNALING	0.377910729	0.999999997
HALLMARK_BILE_ACID_METABOLISM	0.413454301	0.999999997
HALLMARK_HEME_METABOLISM	0.481253969	0.999999997
HALLMARK_UV_RESPONSE_DN	0.52024193	0.999999997
HALLMARK_PI3K_AKT_MTOR_SIGNALING	0.58492227	0.999999997
HALLMARK_HEDGEHOG_SIGNALING	0.58804766	0.999999997
HALLMARK_KRAS_SIGNALING_DN	0.605869514	0.999999997
HALLMARK_ANDROGEN_RESPONSE	0.748988541	0.999999997
HALLMARK_PEROXISOME	0.803261712	0.999999997
HALLMARK_GLYCOLYSIS	0.821549992	0.999999997
HALLMARK_UNFOLDED_PROTEIN_RESPONSE	0.859727268	0.999999997
HALLMARK_FATTY_ACID_METABOLISM	0.862474641	0.999999997
HALLMARK_PROTEIN_SECRETION	0.869307435	0.999999997
HALLMARK_ALLOGRAFT_REJECTION	0.886954491	0.999999997
HALLMARK_P53_PATHWAY	0.904334185	0.999999997
HALLMARK_ANGIOGENESIS	0.909348451	0.999999997
HALLMARK_IL6_JAK_STAT3_SIGNALING	0.914068939	0.999999997
HALLMARK_REACTIVE_OXIGEN_SPECIES_PATHWAY	0.922475651	0.999999997
HALLMARK_APICAL_SURFACE	0.928490118	0.999999997
HALLMARK_IL2_STAT5_SIGNALING	0.959439771	0.999999997
HALLMARK_UV_RESPONSE_UP	0.967586043	0.999999997
HALLMARK_ESTROGEN_RESPONSE_LATE	0.972020235	0.999999997
HALLMARK_XENOBIOTIC_METABOLISM	0.979705067	0.999999997
HALLMARK_COMPLEMENT	0.99032617	0.999999997
HALLMARK_ESTROGEN_RESPONSE_EARLY	0.990701043	0.999999997
HALLMARK_PANCREAS_BETA_CELLS	0.991640362	0.999999997
HALLMARK_KRAS_SIGNALING_UP	0.992024922	0.999999997
HALLMARK_TGF_BETA_SIGNALING	0.99293276	0.999999997
HALLMARK_INFLAMMATORY_RESPONSE	0.995120988	0.999999997
HALLMARK_HYPOXIA	0.998285232	0.999999997
HALLMARK_APICAL_JUNCTION	0.998711642	0.999999997
HALLMARK_TNFA_SIGNALING_VIA_NFKB	0.998906247	0.999999997
HALLMARK_INTERFERON_ALPHA_RESPONSE	0.99980783	0.999999997
HALLMARK_INTERFERON_GAMMA_RESPONSE	0.999847467	0.999999997
HALLMARK_APOPTOSIS	0.999915392	0.999999997
HALLMARK_MTORC1_SIGNALING	0.999986277	0.999999997
HALLMARK_COAGULATION	0.999991192	0.999999997
HALLMARK_EPITHELIAL_MESENCHYMAL_TRANSITION	0.999999972	0.999999997
HALLMARK_CHOLESTEROL_HOMEOSTASIS	0.999999997	0.999999997

Supplementary table 12| Gene sets increased after ten days in 2D hskMP culture exposed to aged human serum compared to the young human serum. Data are derived from hskMPs exposed to human serum from n=3 different young or aged donors. GST Pval = Wilcoxon gene set test p-value. GST FDR = Adjusted p-value using the Benjamini-Hochberg procedure.

Gene Set Name: Human - D4 - *in-vitro*	**GST_Pval**	**GST_FDR**
HALLMARK_OXIDATIVE_PHOSPHORYLATION	2.37546E-27	1.18773E-25
HALLMARK_MYC_TARGETS_V1	9.99263E-21	2.49816E-19
HALLMARK_MTORC1_SIGNALING	1.85244E-17	3.0874E-16
HALLMARK_FATTY_ACID_METABOLISM	4.28616E-13	5.3577E-12
HALLMARK_ADIPOGENESIS	7.65179E-12	7.65179E-11
HALLMARK_EPITHELIAL_MESENCHYMAL_TRANSITION	1.62655E-10	1.35546E-09
HALLMARK_REACTIVE_OXIGEN_SPECIES_PATHWAY	1.02231E-07	7.30222E-07
HALLMARK_GLYCOLYSIS	1.36731E-07	8.54569E-07
HALLMARK_HYPOXIA	6.2757E-07	3.4865E-06
HALLMARK_XENOBIOTIC_METABOLISM	7.87998E-07	3.93999E-06
HALLMARK_CHOLESTEROL_HOMEOSTASIS	1.31717E-06	5.98715E-06
HALLMARK_APOPTOSIS	3.66435E-06	1.52681E-05
HALLMARK_PROTEIN_SECRETION	6.28291E-06	2.4165E-05
HALLMARK_HEME_METABOLISM	1.03897E-05	3.71061E-05
HALLMARK_PEROXISOME	6.94786E-05	0.000231595
HALLMARK_ALLOGRAFT_REJECTION	7.88859E-05	0.000246518
HALLMARK_ESTROGEN_RESPONSE_LATE	0.000119831	0.000352445
HALLMARK_ESTROGEN_RESPONSE_EARLY	0.000144241	0.000400668
HALLMARK_P53_PATHWAY	0.000224146	0.000589858
HALLMARK_PI3K_AKT_MTOR_SIGNALING	0.000250558	0.000626395
HALLMARK_COAGULATION	0.000275532	0.000656028
HALLMARK_ANDROGEN_RESPONSE	0.0009998	0.002272272
HALLMARK_UV_RESPONSE_UP	0.0011426	0.002483913
HALLMARK_UNFOLDED_PROTEIN_RESPONSE	0.003074825	0.00633007
HALLMARK_DNA_REPAIR	0.003165035	0.00633007
HALLMARK_COMPLEMENT	0.004506768	0.008666861
HALLMARK_BILE_ACID_METABOLISM	0.00682946	0.012647149
HALLMARK_MYC_TARGETS_V2	0.011757726	0.020995939
HALLMARK_IL6_JAK_STAT3_SIGNALING	0.016743553	0.028868194
HALLMARK_TGF_BETA_SIGNALING	0.027865236	0.04644206
HALLMARK_INTERFERON_GAMMA_RESPONSE	0.032846143	0.052850754
HALLMARK_TNFA_SIGNALING_VIA_NFKB	0.033824482	0.052850754
HALLMARK_IL2_STAT5_SIGNALING	0.039946673	0.060525262
HALLMARK_PANCREAS_BETA_CELLS	0.059846482	0.088009533
HALLMARK_APICAL_JUNCTION	0.080587632	0.113823879
HALLMARK_INFLAMMATORY_RESPONSE	0.081953193	0.113823879
HALLMARK_INTERFERON_ALPHA_RESPONSE	0.090292878	0.122017402
HALLMARK_ANGIOGENESIS	0.133689274	0.175906939
HALLMARK_E2F_TARGETS	0.219615085	0.281557801
HALLMARK_APICAL_SURFACE	0.245188044	0.306485055
HALLMARK_G2M_CHECKPOINT	0.37068282	0.452052219
HALLMARK_NOTCH_SIGNALING	0.476186059	0.566888165
HALLMARK_UV_RESPONSE_DN	0.497807442	0.578845863
HALLMARK_KRAS_SIGNALING_UP	0.51070201	0.580343194
HALLMARK_HEDGEHOG_SIGNALING	0.691028537	0.767809485
HALLMARK_SPERMATOGENESIS	0.844964205	0.918439353
HALLMARK_WNT_BETA_CATENIN_SIGNALING	0.87252442	0.928217468
HALLMARK_MITOTIC_SPINDLE	0.907292211	0.945096053
HALLMARK_MYOGENESIS	0.983453569	0.99992619
HALLMARK_KRAS_SIGNALING_DN	0.99992619	0.99992619

Supplementary table 13 | Gene sets decreased after four days in 2D hskMP culture exposed to aged human serum compared to the young human serum. Data are derived from hskMPs exposed to human serum from n=3 different young or aged donors. GST Pval = Wilcoxon gene set test p-value. GST FDR = Adjusted p-value using the Benjamini-Hochberg procedure.

Gene Set Name: Human - D10 - *in-vitro*	**GST_Pval**	**GST_FDR**
HALLMARK_CHOLESTEROL_HOMEOSTASIS	3.38115E-09	1.69057E-07
HALLMARK_EPITHELIAL_MESENCHYMAL_TRANSITION	2.8198E-08	7.0495E-07
HALLMARK_COAGULATION	8.80894E-06	0.000146816
HALLMARK_MTORC1_SIGNALING	1.37243E-05	0.000171553
HALLMARK_APOPTOSIS	8.46158E-05	0.000846158
HALLMARK_INTERFERON_GAMMA_RESPONSE	0.000152545	0.001271212
HALLMARK_INTERFERON_ALPHA_RESPONSE	0.000192191	0.001372792
HALLMARK_TNFA_SIGNALING_VIA_NFKB	0.001093828	0.006836424
HALLMARK_APICAL_JUNCTION	0.001288447	0.007158037
HALLMARK_HYPOXIA	0.001714879	0.008574394
HALLMARK_INFLAMMATORY_RESPONSE	0.00487935	0.022178864
HALLMARK_TGF_BETA_SIGNALING	0.00706795	0.029449793
HALLMARK_KRAS_SIGNALING_UP	0.007975567	0.029861084
HALLMARK_PANCREAS_BETA_CELLS	0.008361104	0.029861084
HALLMARK_ESTROGEN_RESPONSE_EARLY	0.009299486	0.030232521
HALLMARK_COMPLEMENT	0.009674407	0.030232521
HALLMARK_XENOBIOTIC_METABOLISM	0.020296026	0.059694193
HALLMARK_ESTROGEN_RESPONSE_LATE	0.027981149	0.077725414
HALLMARK_UV_RESPONSE_UP	0.032415584	0.085304169
HALLMARK_IL2_STAT5_SIGNALING	0.040562078	0.101405195
HALLMARK_APICAL_SURFACE	0.071516386	0.170277109
HALLMARK_REACTIVE_OXIGEN_SPECIES_PATHWAY	0.07752997	0.176204476
HALLMARK_IL6_JAK_STAT3_SIGNALING	0.085936579	0.186818651
HALLMARK_ANGIOGENESIS	0.090659734	0.188874445
HALLMARK_P53_PATHWAY	0.095669122	0.191338244
HALLMARK_ALLOGRAFT_REJECTION	0.113050418	0.217404651
HALLMARK_PROTEIN_SECRETION	0.130698452	0.241859331
HALLMARK_FATTY_ACID_METABOLISM	0.137530456	0.241859331
HALLMARK_UNFOLDED_PROTEIN_RESPONSE	0.140278412	0.241859331
HALLMARK_GLYCOLYSIS	0.178455331	0.297425551
HALLMARK_PEROXISOME	0.196746281	0.317332711
HALLMARK_ANDROGEN_RESPONSE	0.251020589	0.39221967
HALLMARK_KRAS_SIGNALING_DN	0.394140878	0.592983711
HALLMARK_HEDGEHOG_SIGNALING	0.411971511	0.592983711
HALLMARK_PI3K_AKT_MTOR_SIGNALING	0.415088598	0.592983711
HALLMARK_UV_RESPONSE_DN	0.479767137	0.666343246
HALLMARK_HEME_METABOLISM	0.518754536	0.701019643
HALLMARK_BILE_ACID_METABOLISM	0.586557064	0.77178561
HALLMARK_NOTCH_SIGNALING	0.622108325	0.797574776
HALLMARK_WNT_BETA_CATENIN_SIGNALING	0.681572497	0.844519472
HALLMARK_DNA_REPAIR	0.692505967	0.844519472
HALLMARK_ADIPOGENESIS	0.753701485	0.887042534
HALLMARK_SPERMATOGENESIS	0.76285658	0.887042534
HALLMARK_MITOTIC_SPINDLE	0.806488121	0.916463774
HALLMARK_MYOGENESIS	0.925794414	0.999999764
HALLMARK_MYC_TARGETS_V2	0.970438614	0.999999764
HALLMARK_G2M_CHECKPOINT	0.991507212	0.999999764
HALLMARK_E2F_TARGETS	0.996540502	0.999999764
HALLMARK_MYC_TARGETS_V1	0.999044493	0.999999764
HALLMARK_OXIDATIVE_PHOSPHORYLATION	0.999999764	0.999999764

Supplementary table 14 | Gene sets decreased after ten days in 2D hskMP culture exposed to aged human serum compared to the young human serum. Data are derived from hskMPs exposed to human serum from n=3 different young or aged donors. GST Pval = Wilcoxon gene set test p-value. GST FDR = Adjusted p-value using the Benjamini-Hochberg procedure.